

Simulation of Hurricane Harvey flood event through coupled hydrologic-hydraulic models: Challenges and next steps

Tigstu T. Dullo¹ | Sudershan Gangrade^{2,3,4}  | Mario Morales-Hernández^{4,5} |
Md Bulbul Sharif⁶ | Shih-Chieh Kao^{2,3,4}  | Alfred J. Kalyanapu¹  |
Sheikh Ghafoor⁶ | Katherine J. Evans^{2,4,5}

¹Department of Civil and Environmental Engineering, Tennessee Technological University, Cookeville, Tennessee

²The Bredesen Center, University of Tennessee, Knoxville, Tennessee

³Environmental Sciences Division, Oak Ridge National Laboratory, Oak Ridge, Tennessee

⁴Climate Change Science Institute, Oak Ridge National Laboratory, Oak Ridge, Tennessee

⁵Computational Sciences and Engineering Division, Oak Ridge National Laboratory, Oak Ridge, Tennessee

⁶Department of Computer Science, Tennessee Technological University, Cookeville, Tennessee

Correspondence

Alfred J. Kalyanapu, PhD, 1020 Stadium Drive, P O Box 5015, Cookeville, TN 38505.
Email: akalyanapu@tnstate.edu

Funding information

Funded by US Air Force Numerical Weather Modeling Program.

Abstract

Using the 2017 Hurricane Harvey flood event as a test case, this study set up a series of sensitivity analyses to highlight three challenges associated with large-scale flood inundation modeling, including (a) model parameterization, (b) errors in digital elevation models, and (c) effects of reservoir retention. Driven by radar-based hourly rainfall data, a series of hydrologic-hydraulic models including the VIC hydrologic model, RAPID routing model, and Flood2D-GPU hydrodynamic model are set up over Harris County, Texas, to simulate flood inundation and hazards. The results demonstrate the importance of hydrologic parameters in improving flood modeling. For a large flood event such as Hurricane Harvey, the effect of the initial water depths is insignificant. The Manning's n values may increase the peak water depth by ~1%, the flood extents by 65km^2 , and the high danger zone by ~6%. On the contrary, the bathymetry correction factors may reduce the flood extent by ~1.4% and the high-danger zone by ~4%. Reducing the reservoir storage capacity to 1% may increase the flood extent by ~4% and the high-danger zone by ~17%. This

Notice: This manuscript has been authored by UT-Battelle, LLC, under contract DE-AC05-00OR22725 with the US Department of Energy (DOE). The US government retains and the publisher, by accepting the article for publication, acknowledges that the US government retains a nonexclusive, paid-up, irrevocable, worldwide license to publish or reproduce the published form of this manuscript, or allow others to do so, for US government purposes. DOE will provide public access to these results of federally sponsored research in accordance with the DOE Public Access Plan (<http://energy.gov/downloads/doe-public-access-plan>).

This is an open access article under the terms of the Creative Commons Attribution-NonCommercial-NoDerivs License, which permits use and distribution in any medium, provided the original work is properly cited, the use is non-commercial and no modifications or adaptations are made.

© 2021 Oak Ridge National Laboratory, managed by UT-Battelle, LLC. *Journal of Flood Risk Management* published by Chartered Institution of Water and Environmental Management and John Wiley & Sons Ltd.

study may provide supporting information to guide and prioritize the development of future high-performance computing hydrodynamic large-scale flood simulations.

KEY WORDS

digital elevation model (DEM), flood simulation, graphics processing unit (GPU), Hurricane Harvey, model parameterization, reservoir

1 | INTRODUCTION

Floods are costly and destructive natural disasters resulting in casualties, population displacement, infrastructure damage, and economic losses (UNISDR, 2015). Severe flood events can span across different spatial scales and can last from days to months, having significant impacts upon society. Clearly, our ability to conduct spatially explicit simulations of flood regimes at high resolution (Nardi, Annis, Di Baldassarre, Vivoni, & Grimaldi, 2019; Zheng, Maidment, Tarboton, Liu, & Passalacqua, 2018), large spatial extent (Nardi, Biscarini, Francesco, Manciola, & Ubertini, 2013; Sampson et al., 2015; Wing et al., 2017), and long temporal duration in a timely manner (Emerton et al., 2016; Schumann et al., 2013; Wing et al., 2019) is critical in determining the impacts and risks associated to these events.

However, process-based simulation of flood regimes is not a trivial task. It requires coupling of a series of atmospheric, hydrologic, and hydraulic data/models that includes several processes spanning across the water cycle (Grimaldi, Schumann, Shokri, Walker, & Pauwels, 2019; Sampson et al., 2015). The four major assessment steps include input rainfall data preparation, runoff estimation, streamflow simulation, and flood inundation modeling. Each step involves data/models with different complexities, input requirements, and computational demands and is studied by different research disciplines. Among these major modeling steps, inundation modeling requires a much finer time step and spatial resolution and hence has been a computational bottleneck in the coupled hydrologic-hydraulic modeling chain (Getirana, Peters-Lidard, Rodell, & Bates, 2017; Peña & Nardi, 2018).

Although there are simplified approaches, such as geomorphic floodplain modeling (Annis, Nardi, Morrison, & Castelli, 2019; Liu, Maidment, Tarboton, Zheng, & Wang, 2018; Manfreda et al., 2014; Nardi et al., 2019; Nardi, Vivoni, & Grimaldi, 2006) for efficient approximation, process-based understanding requires 1D or 2D hydrodynamic models that are computationally intensive for large-scale applications. With advances in computer technology, this computational limitation is being

resolved (Bates, Horritt, & Fewtrell, 2010; Kalyanapu, Shankar, Pardyjak, Judi, & Burian, 2011; Morales-Hernández et al., 2020; Neal, Schumann, & Bates, 2012). Enhanced computing power has enabled large-scale flood modeling applications ranging from regional to national scales (Sampson et al., 2015; Wing et al., 2017; Wing et al., 2019). However, although higher-resolution (i.e., 10 m or finer spatial resolution) flood modeling studies are being reported in the recent literature (Noh, Lee, Lee, & Seo, 2019; Nyaupane et al., 2018), there are various open challenges for large-scale flood simulation. Some of the challenges in a large-scale coupled hydrologic-hydraulic modeling framework are (a) high computational cost for model tuning and calibration (model parameterization), even with the support of high-performance computing (HPC) (Dung, Merz, Bárdossy, Thang, & Apel, 2011; Getirana et al., 2017; Peña & Nardi, 2018), (b) inaccuracy in digital elevation models (DEMs) (Bhuyian, Kalyanapu, & Nardi, 2014; Casas, Benito, Thorndycraft, & Rico, 2006; Cook & Merwade, 2009; McKean, Tonina, Bohn, & Wright, 2014), and (c) difficulty in addressing reservoir operation and regulation (Fleischmann, Collischonn, Paiva, & Tucci, 2019; Mateo et al., 2014; Shin, Pokhrel, & Miguez-Macho, 2017). These open challenges demand more focused research efforts that cannot be resolved simply by enhanced computational capacity (Grimaldi et al., 2019).

For model parameterization, it is important to understand the sensitivity of selected hydrologic and hydraulic parameters, including, but not limited to, rainfall, initial soil moisture condition, Manning's roughness coefficient (Manning's *n* value), and initial water depth, to quantify and compare their respective influences. Rainfall depth can be taken from observations (e.g., radar-based Stage IV Quantitative Precipitation Estimate [ST4; Lin, 2011]) or events simulated by operational weather forecasting models or downscaled Earth system models, each with different levels of uncertainty. Similarly, the initial soil moisture condition is known as a sensitive parameter in hydrologic models and is essential in improving flood model predictions (Massari et al., 2014; Massari, Brocca, Moramarco, Tramblay, & Didon Lescot, 2014). Hydraulic

parameters such as the initial water depth and Manning's n values are also vital parameters for accurate estimation of flood model results (Lim & Brandt, 2019). While the effects of these individual parameters have been heavily studied (Aronica, Bates, & Horritt, 2002; Pappenberger, Beven, Horritt, & Blazkova, 2005), their relative sensitivity in the context of large-scale flood inundation modeling needs further exploration.

The other challenge in large-scale flood inundation modeling is the accuracy of DEM (Bhuyian et al., 2014). The DEM, which is used to represent floodplain and channel bathymetry, is one of the most important input data that determines the accuracy of flood model results (Casas et al., 2006; Cea & French, 2012; Conner & Tonina, 2014; Cook & Merwade, 2009; Horritt, 2006; McKean et al., 2014). One of the biggest challenges is that most existing DEM products provide water surface elevation, not the channel bathymetry needed by hydraulic models (Bhuyian et al., 2014). In addition, the accuracy of the base DEM is also impacted by features such as vegetation canopies, levees, elevated roads and bridges (Baugh, Bates, Schumann, & Trigg, 2013; Nardi, Morrison, Annis, & Grantham, 2018; Rudorff, Melack, & Bates, 2014; Scheel, Morrison, Annis, & Nardi, 2019; Yamazaki et al., 2012). Although the accuracy of DEM can be improved by correcting it with a river channel profile measured in an on-site survey, that process is also very expensive and problematic for large-scale implementation.

One further challenge in large-scale flood modeling is the difficulty in addressing reservoir operation and regulation. To fully address the effects of reservoir regulation in hydrologic-hydraulic simulation, hydrologic routing and inundation models need to be dynamically coupled with a reservoir operation model (Fleischmann et al., 2019; Mateo et al., 2014; Shin et al., 2017), which involves a heavy investment in software development. In addition, a reservoir management model can perform well only when the operators fully follow the operation guide curves; whereas, the actual operation often deviates from guide curves given different event specific considerations. Due to the modeling complexity and data limitations, there has not been a widely accepted way to include reservoir operation in the coupled hydrologic-hydraulic models. As a result, the effect of reservoir regulation has remained an open challenge and has not been resolved in large-scale flood simulation.

To highlight the main challenges associated with large-scale coupled hydrologic-hydraulic modeling simulation, we used Hurricane Harvey as a test case in this study. Hurricane Harvey, which made landfall on August 25, 2017, near Houston, Texas, was one of the most destructive storms in US history. It impacted millions of

people and resulted in immense property damage in the southeastern part of Texas (Bass, O'Connor, & Perotin, 2018; HCFCD, 2018; Sebastian et al., 2017). Given the Hurricane Harvey flood event's rareness and complexity, it can serve as a suitable test case to explore and identify issues associated with large-scale flood simulation. If a modeling framework can reasonably simulate this major flood event, it should be applicable to simulating most other large-scale flood events with similar drivers for broader applications.

To replicate the Hurricane Harvey flood event, we first used the radar-based hourly ST4 rainfall data to drive the Variable Infiltration Capacity (VIC) hydrologic model (VIC; Liang, Lettenmaier, Wood, & Burges, 1994). The simulated runoff was routed using the Routing Application for Parallel computation of Discharge (RAPID) through the National Hydrography Dataset Plus (NHD; McKay et al., 2012) river network. A high-resolution graphics processing unit (GPU)-accelerated flood model, Flood2D-GPU (Morales-Hernández et al., 2020), was then set up over a large domain ($6,550 \text{ km}^2$) in Harris County, Texas, at a high spatial resolution (10 m, with a total of ~68 million computing cells). After model evaluation, we tested and compared flood inundation responses associated with different model parameterizations and DEM accuracies, as well as reservoir flood retention capacity. We then evaluated the overall modeling challenges and priorities for future coupled hydrologic-hydraulic model enhancement for the purpose of large-scale flood inundation simulation.

This paper is organized as follows: the data and methods are discussed in Section 2; Section 3 presents the result and discussion; and the summary is presented in Section 4.

2 | DATA AND METHODS

2.1 | Study area

Harris County (Figure 1), located in the southeastern part of the state of Texas in the United States and covering the Houston metropolitan area, is the focus of this study. This region is mainly overlapped by two eight-digit Hydrologic Unit Code (HUC08) sub basins (12,040,102: Spring and 12,040,104: Buffalo-San Jacinto) with a total drainage area of ~5,000 km^2 . It combines with two other HUC08 tributaries (12,040,101: West Fork San Jacinto and 12,040,103: East Fork San Jacinto) to form the San Jacinto River Basin (a six-digit HUC: 120401) that drains into Galveston Bay either through the San Jacinto River or through the Houston Ship Channel (Buffalo Bayou) (Storey & Talbott, 2009). Flooding is the most

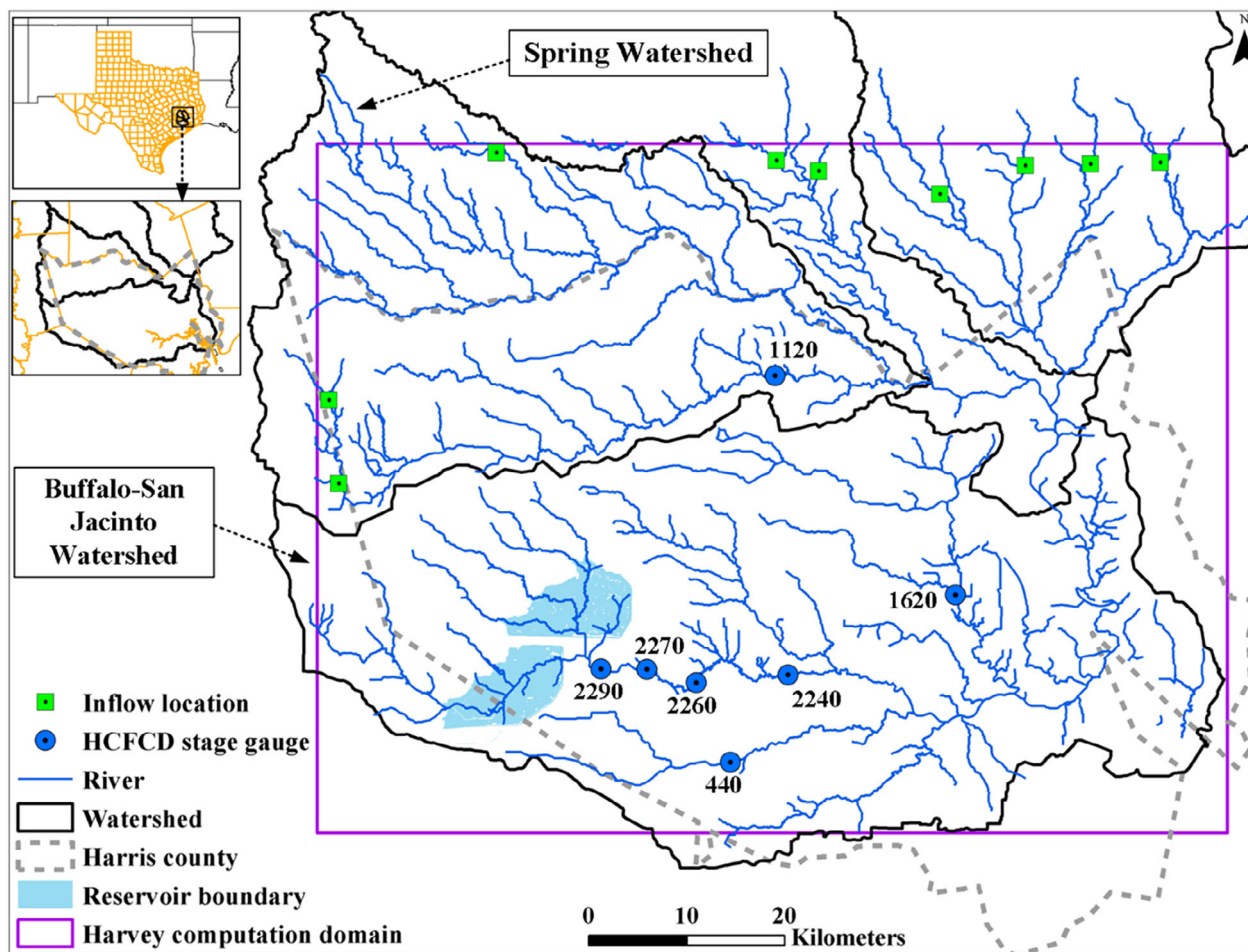


FIGURE 1 Harris County study area location

frequent natural disaster in Harris County (HCFCD, 2016; HCFCD, 2018). At the very least, a part of the county experiences major floods in about every 2 years (HCFCD, 2018). To reduce the flood risk along Buffalo Bayou and the City of Houston, the US Army Corps of Engineers (USACE) built the Addicks (357.4 km^2) and Barker (326.3 km^2) reservoirs (Figure 1) in the 1940s (USACE, 2012).

2.2 | Model setup

2.2.1 | Rainfall input

We used the National Center for Environmental Prediction 4 km spatial resolution hourly ST4 rainfall data to drive the hydrologic-hydraulic model simulation for the Hurricane Harvey flood event. ST4 is radar-based rainfall estimates with corrections based on rain gauges and quality control by National Weather Service River Forecast Centers. It has been used in various applications, such as flood forecasting, numerical weather model verification, and

extreme rainfall analysis (Kao, DeNeale, & Watson, 2019; Luitel, Villarini, & Vecchi, 2018; Nelson, Prat, Seo, & Habib, 2016; Prat & Nelson, 2015). ST4 features spatial rainfall distributions detected by weather radar that cannot be measured by conventional gauge networks. For Hurricane Harvey, Kao et al. (2019) evaluated the reasonableness of ST4 using 153 rain gauges in Harris County and found high R^2 values between hourly rain gauge observations and ST4. Further discussion of ST4 and its intercomparison with other precipitation products can be found in Gourley, Hong, Flamig, Li, and Wang (2010). The ST4 rainfall data is bilinearly interpolated to the hydrologic modeling grids for the runoff and streamflow simulation. Given the overall smooth terrain in the study area, the orographic effects on rainfall is small and hence topography is not considered in the interpolation.

2.2.2 | Runoff and streamflow modeling

A $1/24^\circ$ ($\sim 4 \text{ km}$) -resolution VIC model implementation from Oubeidillah, Kao, Ashfaq, Naz, and Tootle (2014)

and Naz et al. (2016) was used to simulate runoff driven by ST4 rainfall. To support large-scale hydroclimate assessment, Oubeidillah et al. (2014) provided pre-organized VIC parameters that were calibrated for 2,107 HUC08s across the conterminous US (CONUS) using the US Geological Survey (USGS) WaterWatch runoff data set (Brakebill, Wolock, & Terziotti, 2011). To cover all 1929 river segments (from NHD+) and tributaries in the San Jacinto River Basin, we conducted VIC simulation for all four HUC08s (12040101–12040104) in the San Jacinto River Basin. The hourly ST4 rainfall data were spatially interpolated to each VIC grid cell for hourly simulation. The simulated hourly VIC total runoff was then routed through 1929 NHD+ river segments in the San Jacinto River Basin by RAPID to simulate streamflow (similar to the procedures used in Forbes et al., 2019). The detailed model evaluation results are presented and discussed in Section 3.1.

2.2.3 | Inundation modeling

Inundation modeling was performed using the computationally enhanced version of Flood2D-GPU (Morales-Hernández et al., 2020) that allows parallel computing using multiple GPU cards through a hybrid message passing interface (MPI) and Compute Unified Device Architecture (CUDA). The numerical algorithm used in this version of Flood2D-GPU solves nonlinear hyperbolic shallow water equations using an upwind finite-volume explicit scheme, based on Roe's linearization. The shallow water equations are a simplified version of the Navier-Stokes equations, representing the continuity and the depth-averaged horizontal momentum equations (see Morales-Hernández et al. (2020) for further model details).

To replicate the Hurricane Harvey flood event, we used a one-third arc-second (~10 m) spatial resolution National Elevation Dataset (NED) DEM from the USGS (Archuleta et al., 2017). The DEM layers are derived from data sources such as Light Detection and Ranging (LIDAR), Interferometric Synthetic Aperture Radar (IFSAR), or from photogrammetric technologies like image correlation and manual profiling by edge matching and mosaicking elevation data (Archuleta et al., 2017; Sugarbaker et al., 2014). To improve the quality of the base DEM, we removed elevated roads and bridges that could obstruct the flow of water in some of the streams and rivers. The Flood2D-GPU simulation was set up for the Harvey computation domain in Figure 1, which has an approximate area of 6,550 km² and includes ~68 million model grid cells (7,183 rows × 9,478 columns in a uniform structured mesh). We conducted flood simulation for a 10-day period from August 25 to September

3, 2017. To input streamflow from RAPID to Flood2D-GPU, we selected 9 inflow locations (Figure 1) along the boundary of the computation domain and used the NHD + river network to couple both models (following a similar procedure to that used in Gangrade, Kao, Dullo, Kalyanapu, & Preston, 2019). For the rest of the computation domain, runoff hydrographs from the VIC model were input to Flood2D-GPU using VIC grid map. In this study, the hydraulic and geometric parameters from the calibration section (Section 3.1) were used in conjunction with the base case scenarios for rainfall depth and initial soil moisture conditions in the flood simulation. The downstream boundary condition was set to 0.10 Froude number that has been estimated for a bay area (da Silva, Buijsman, & Magalhaes, 2015). The simulation was conducted using the Summit supercomputer managed by the Oak Ridge Leadership Computing Facility, which relies heavily on GPUs to greatly accelerate scientific computation. The evaluation of Flood2D-GPU performance is presented and discussed in Section 3.1.

2.3 | Sensitivity analysis

Among various challenges associated with large-scale flood simulation, in this study we focused on three aspects related to inundation modeling: (a) model parameterization, (b) DEM accuracy, and (c) effects of reservoir flood retention. We set up a series of sensitivity analyses to quantify and compare their respective influences. The tested hydrologic and hydraulic parameters (i.e., precipitation, soil moisture condition, Manning's *n* value, and initial water depth), river bathymetry correction factors, and reservoir storage capacity in each scenario are summarized in Table 1.

To select ranges for the initial water depth, we summarized the observed water depth values before the flood events that were used in the calibration and validation. In this study, the calibration and validation of the flood model were performed using the flood event from April 17 to 18, 2016 (which is also known as the "Tax Day" flood event) and the Hurricane Harvey flood event, respectively. The distribution of observed water depth values (Figure 2a) from 115 Harris County Flood Control District (HCFCD) gauges, before Tax Day flood event, showed that ~75% had values between 0.0 and 0.20 m. Similar trends were found before the Hurricane Harvey flood event, where ~50% of the gauges had water depth values between 0.0 and 0.50 m. As a result, we selected initial water depth values ranging from 0.0 to 0.50 m (Table 1) for the model calibration and sensitivity analysis. The Manning's *n* value map for the Harris County flood model (Figure 3) was prepared based on the

TABLE 1 Summary of hydrologic and hydraulic parameters used in the sensitivity analysis

Sensitivity parameter	Scenario	Initial water depth values (m)	Manning's <i>n</i> values	Bathymetry correction factor (m)	Reservoir storage capacity	Precipitation	Soil moisture
Precipitation	1	0.20	N_2 = decreased by 10%	-1.50	100.00%	P_1 = increased by 10%	Base case
	2					P_2 = increased by 5%	
	3					P_3 = base case	
	4					P_4 = decreased by 5%	
	5					P_5 = decreased by 10%	
Soil moisture	1	0.20	N_2 = decreased by 10%	-1.50	100.00%	Base case	SM_1 = increased by 10%
	2						SM_2 = increased by 5%
	3						SM_3 = base case
	4						SM_4 = decreased by 5%
	5						SM_5 = decreased by 10%
Initial water depth	1	0.000	N_2 = decreased by 10%	-1.50	100.00%	Base case	Base case
	2	0.200					
	3	0.300					
	4	0.400					
	5	0.500					
Surface roughness	1	0.20	N_1 = decreased by 20%	-1.50	100.00%	Base case	Base case
	2		N_2 = decreased by 10%				
	3		N_3 = base case				
	4		N_4 = increased by 10%				
	5		N_5 = increased by 20%				
Bathymetry correction factor	1	0.20	N_2 = decreased by 10%	0.00	100.00%	Base case	Base case
	2			-0.75			
	3			-1.50			
	4			-2.00			
	5			-2.50			
Reservoir storage capacity	1	0.20	N_2 = decreased by 10%	-1.50	100.00%	Base case	Base case
	2				75.00%		
	3				50.00%		
	4				30.00%		
	5				20.00%		
	6				10.00%		
	7				1.00%		

Note: For the Manning's *n* value, N_3 (i.e., Base case) is prepared based on the NLCD 2011.

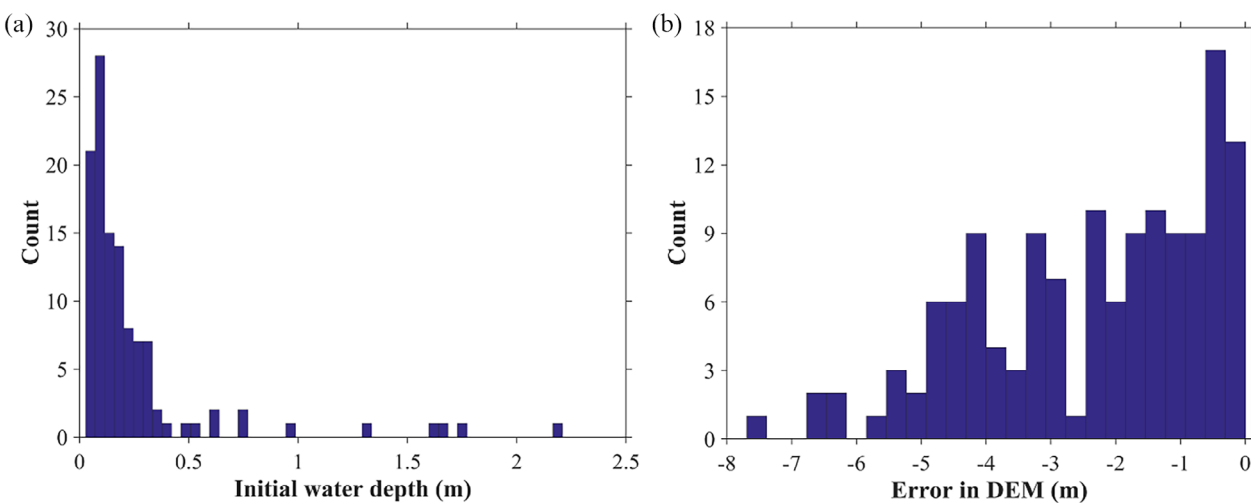


FIGURE 2 Histogram plots for (a) observed initial water depth values, and (b) error in DEM

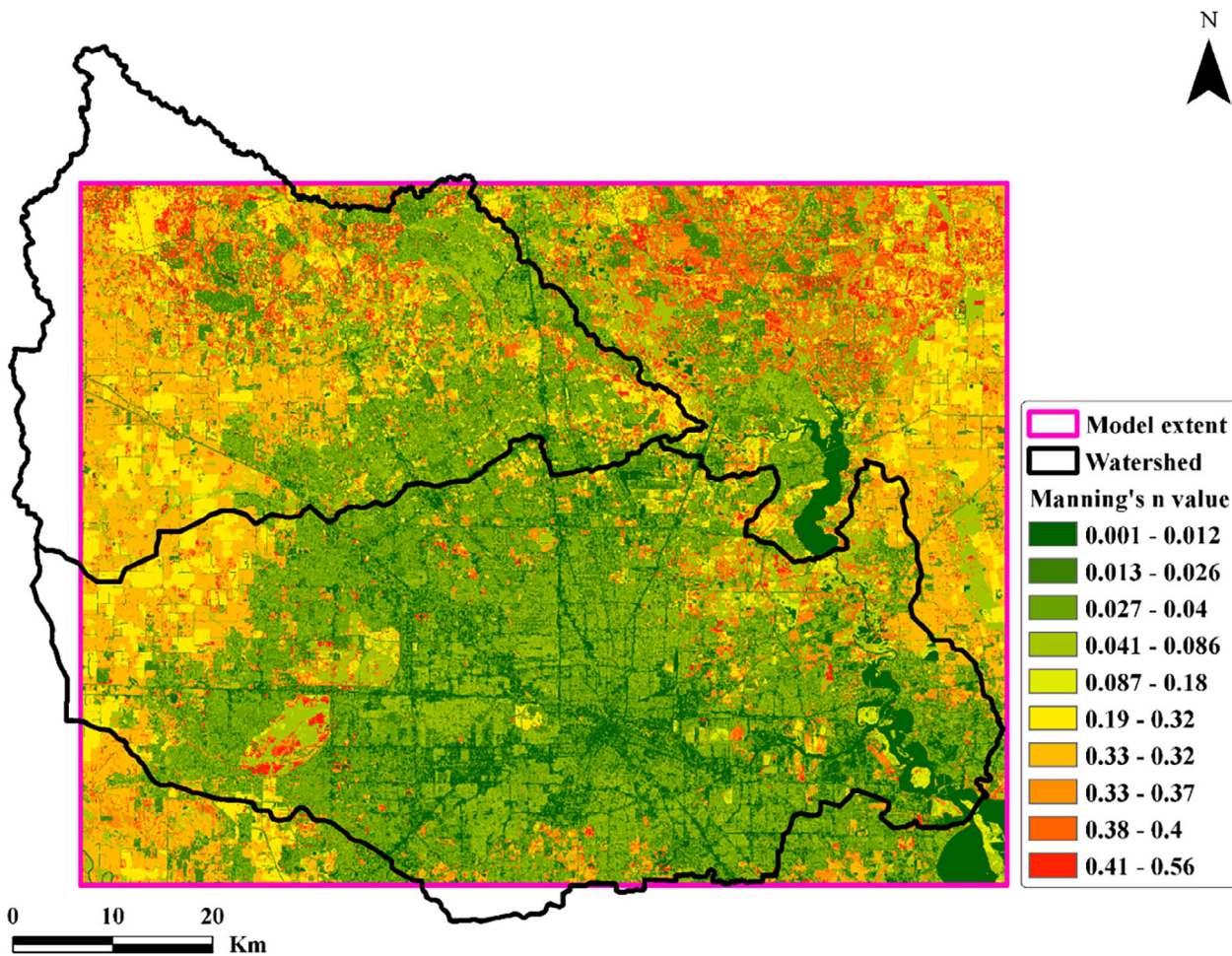


FIGURE 3 Manning's *n* value map for Harris County flood model

National Land Cover Dataset (NLCD) 2011 (MRLC, 2011) following the approach used by Kalyanapu, Burian, and McPherson (2010). To assess the

relative sensitivity of the model output to the Manning's *n* values, we selected four scenarios within $\pm 20\%$ range (Table 1).

TABLE 2 Summary of utilized computing hours, number of GPUs, and output file size of the Flood2D-GPU simulation

Simulation	Number of simulations	Number of HPC nodes and GPUs per simulation ^a	Total computing time (hours)	Output file size at a 30-min interval (Terabyte)	Output file format
Tax Day Flood (model calibration)	10	8 nodes (48 GPUs)	1.5/simulation (15 total)	15.0	Binary
Hurricane Harvey (model validation)	1	8 nodes (48 GPUs)	1.5	0.7	Binary
Hurricane Harvey (sensitivity analysis)	32	8 nodes (48 GPUs)	1.5/simulation (48 total)	23.0	Binary

^aThis study used OLCF Summit supercomputer. Each Summit node has 6 NVIDIA Volta GPUs (<https://www.olcf.ornl.gov/summit/>).

To understand the issue of DEM accuracy in the Hurricane Harvey flood simulation, we looked up surveyed channel bottom elevations at 139 locations from HCFCD and compared their corresponding values in the DEM. The error (i.e., measured channel bottom elevation minus DEM elevation) was found to be from -7.85 m to -0.15 m (Figure 2b), indicating that the base DEM was consistently over-estimated. Without incorporating further channel profile information from the on-site survey (because was not feasible for large-scale simulation), we tested various bathymetry correction factors in the sensitivity analysis. Since $\sim 60\%$ of the locations had values between -2.5 m and -0.15 m (Figure 2b), we selected four scenarios ranging from -2.5 m to -0.75 m (Table 1). Based on the flow area information provided by NHD+, with additional manual adjustment using satellite images, we identified the coverage of the main channel regime in the study area. We then reduced the DEM elevation along the river channel cells by selected bathymetry correction factors for the sensitivity analysis. This simple approach is unlikely to adjust the channel bathymetry to the true natural channel elevations. However, the selected values should help us understand the relative sensitivity of channel topography to other controlling factors.

A further sensitivity analysis is designed to demonstrate the effects of reservoir retention capacity on downstream flooding—in particular, the role of the Addicks and Barker Reservoirs in west Harris County. To develop suitable scenarios, we looked up the elevation-capacity curves of the Addicks and Barker Reservoirs provided by USACE (2012). We first constructed the elevation-capacity curves directly from DEMs and compared them with the USACE curves (2012). Given that both reservoirs are mainly purposed for flood control and do not have constant water storage, the comparison between the DEM and USACE curves (2012) yielded consistent results (not shown). Subsequently, we looked up elevations of both the Addicks and Barker Reservoirs corresponding to 75, 50, 30, 20, 10, and 1% of full storage (Table 1). We

eventually lowered the Addicks and Barker dam heights in the DEM and used the adjusted DEM for sensitivity analysis. Through this specific test, we wanted to understand how significant the effects of reservoir retention/operation are for the purpose of flood simulation (i.e., compared with other controlling factors). The results were intended to help us set priorities for the development and enhancement of large-scale flood simulations and understand relative importance of reservoir retention capacity among other factors.

To understand the impacts of the selected sensitivity parameters on flood damage, the simulated flood depths and velocities were used to develop indicative flood hazard maps following the approach used by Kalyanapu, Judi, McPherson, and Burian (2012). Depth-velocity-flood danger level relationships were classified into three zones: low-danger zone (the number of lives in jeopardy is assumed to be zero), judgment zone (zone of uncertainty where judgment is left for the analyst), and high-danger zone (lives are in jeopardy) (ACER, 1988). For more details on the development of flood hazard maps, see Kalyanapu et al. (2012). Additional details about the number of GPUs used, the machine hour required, and output file size generated for intermediate flood depth and velocity maps are presented in Table 2.

3 | RESULTS AND DISCUSSION

3.1 | Model evaluation

3.1.1 | Streamflow

To ensure the accuracy of the coupled VIC and RAPID models, before simulating the Hurricane Harvey flood event, we performed model evaluation using a long-term gridded 1980–2012 meteorological forcing dataset assembled by Daymet (Thornton, Running, & White, 1997), PRISM (Daly et al., 2008), and the North American Regional Reanalysis (Mesinger et al., 2006) by

TABLE 3 Selected USGS gauge stations for streamflow evaluation

HUC08	NWIS ID	Gauge name	Area (km ²)	NSE	
				Monthly	Daily
12,040,101	08068090	W Fk San Jacinto Rv abv Lk Houston nr Porter, TX	2,492	0.74	0.52
12,040,102	08068500	Spring Ck nr Spring, TX	1,059	0.70	0.47
12,040,103	08070500	Caney Ck nr Splendora, TX	272	0.50	0.41
12,040,103	08070200	E Fk San Jacinto Rv nr New Caney, TX	1,005	0.83	0.62
12,040,104	08075000	Brays Bayou at Houston, TX	246	0.82	0.53
12,040,104	08074500	Whiteoak Bayou at Houston, TX	246	0.76	0.56

Abbreviation: NWIS, National Water Information System.

Oubeidillah et al. (2014). Six USGS daily streamflow gauge stations with long-term observations across the study area (1–2 gauges per HUC08) were selected for model evaluation. Since the monthly total runoff had been calibrated by Oubeidillah et al. (2014) and Naz et al. (2016), we further calibrated the two Muskingum routing parameters in RAPID to improve its ability to simulate daily streamflow. Information on the selected gauge stations, along with their monthly and daily Nash-Sutcliffe coefficients and coefficients of determination (R^2) values, are summarized in Table 3.

Overall, the coupled VIC and RAPID models performed satisfactorily in simulating streamflow. Five out of six gauges had monthly Nash-Sutcliffe efficiency (NSE) values greater than 0.74, and four out of six gauges had daily NSE values greater than 0.52. As expected, the Muskingum routing parameters mostly affected the performance of daily streamflow statistics and were not sensitive to monthly streamflow. This result was consistent with our understanding that the hydrologic model (in this case VIC) would have more effect on the long-term water budget, and the streamflow routing model (in this case RAPID) would have more effect on the short-term streamflow timing. A stepwise procedure that first calibrated hydrologic model runoff at a monthly scale and then calibrated streamflow routing at a daily scale seemed to be a reasonable approach in this case. Note that the main purpose of this VIC-RAPID evaluation is to ensure that the hydrologic model can reasonably represent the long-term hydrologic variability and water balance at the monthly and daily scales. The reasonableness of the subdaily model performance will be jointly evaluated by the subdaily river stage in the following section.

3.1.2 | Inundation

To evaluate the performance of Flood2D-GPU, we calibrated and validated the Harris County flood model

using the Tax Day flood event and the Hurricane Harvey flood event, respectively. For the calibration, we selected eight representative river reaches (Figure 4; Table 4) based on the availability of stage gauge stations and watershed coverage. Observed hourly stage hydrographs (April 2 to May 12, 2016), obtained from HCFC, were used to drive the Flood2D-GPU model. A total of about 10 combinations of Flood2D-GPU parameters were tested to select the most suitable initial water depth, Manning's n value map, and bathymetry correction factor. The final selected parameters include an initial water depth value of 0.20 m, a Manning's n value map (i.e., based on NLCD 2011) reduced by 10%, and a bathymetry correction factor of -1.50 m. These parameters are used for Hurricane Harvey flood validation and served as the base values for sensitivity analysis. Given the high computation cost (e.g., a single simulation of the Harris County flood model requires around 1.5 hours computing time and 1.5 terabyte computer disk space [-Table 2]), we did not use an interactive calibration algorithm to optimize the parameters. Such an approach will be more feasible for a smaller study domain. The number of GPUs used, the total computing time, and output file size generated during the calibration are presented in Table 2.

The comparison between the observed and simulated water surface elevation was performed using three statistical measure of fits including NSE, Root Mean Square Error (RMSE)-Observation Standard Deviation Ratio (RSR), and percent bias (PBIAS). The RSR estimates the differences between observed and simulated water surface elevation, while the PBIAS measures the tendency of the model to underestimate or overestimate (da Silva, de Aguiar Netto, et al., 2015; Moriasi et al., 2007). The model evaluation results showed good performance for the majority of stage gauge stations (Figure 4; Table 4), which indicate that the calibrated flood model can be reasonably used for simulating the Hurricane Harvey flooding for Harris County.

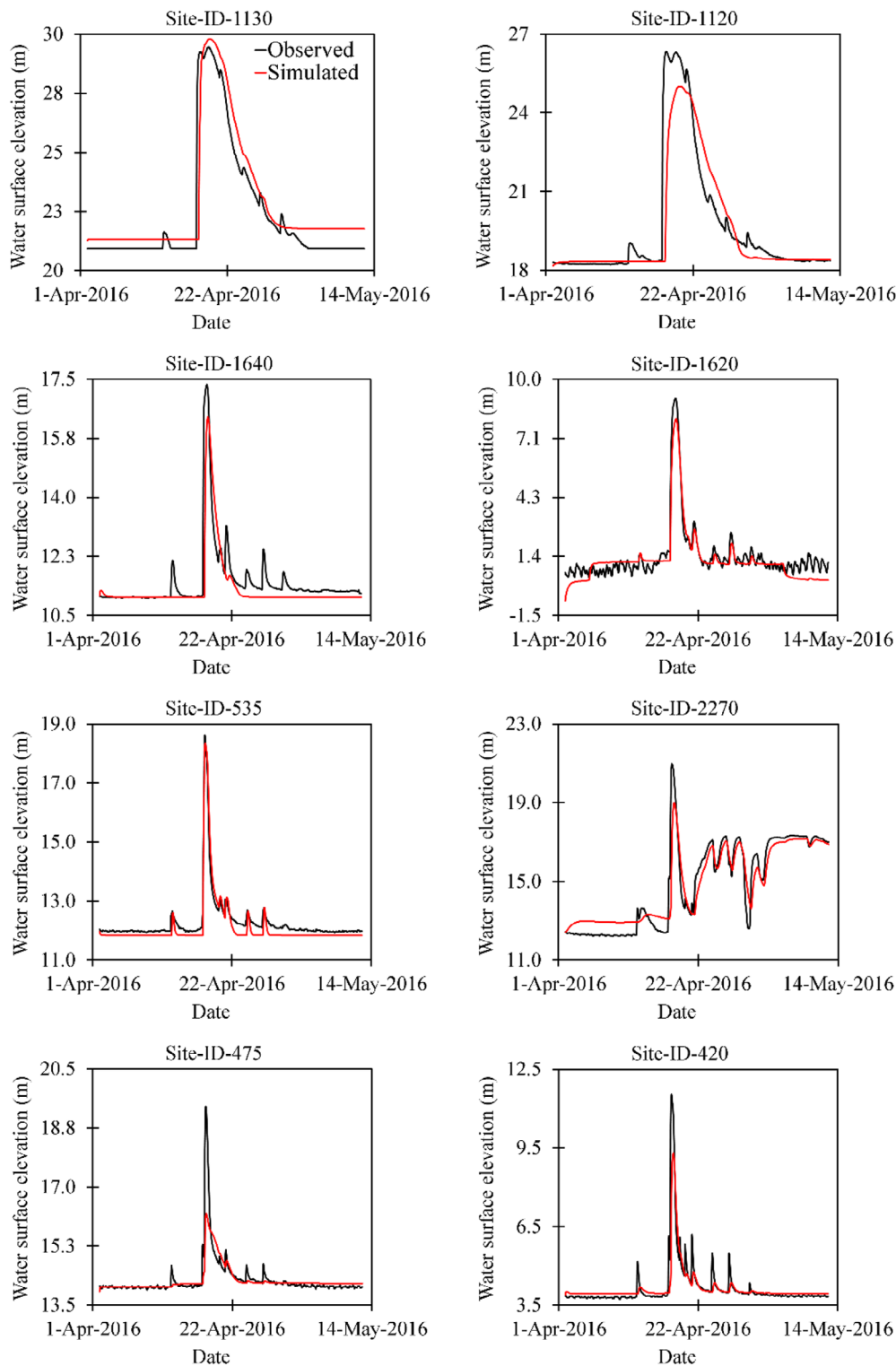


FIGURE 4 A comparison of simulated and observed water surface elevation for flood model calibration period. The HCFCD site IDs and site names can be found in Table 4

To validate the Hurricane Harvey flood simulation results, we compared the modeled outputs with observed stage hydrographs and flood inundation extent derived from observed high water marks. Simulated stage hydrograph extracted at 12 representative gauge locations were compared with observed water surface elevation obtained from HCFCD gauge stations (Figure 5; Table 5). The

results from the validation showed good performance for most of the gauge stations (Table 5), indicating that the Flood2D-GPU model was able to replicate the Hurricane Harvey flood event.

Further, the simulated maximum flood extent was validated by comparing with flood extent derived from observed high water mark points (Watson et al., 2018).

TABLE 4 Tax Day flood calibration results

Upstream limits		Downstream limits						
Site name	HCFCD site ID	Site name	HCFCD site ID	NSE	RSR	PBIAS		
Cypress Creek at Stuebner-Airline Road	1,140	Cypress Creek at Kuykendahl Road	1,130	0.86	0.37	-2.02		
Cypress Creek at Kuykendahl Road	1,130	Cypress Creek at interstate 45	1,120	0.79	0.46	0.62		
Greens Bayou at Beltway 8	1,645	Greens Bayou at U.S. highway 59	1,640	0.65	0.59	1.73		
Greens Bayou at Tidwell Road	1,685	Greens Bayou at Ley Road	1,620	0.89	0.34	11.84		
Halls Bayou at Tidwell Road	1,675	White Oak Bayou at Pinemont Drive	535	0.91	0.29	1.29		
White Oak Bayou at Tidwell Road	575	Buffalo Bayou at West Beltway 8	2,270	0.88	0.34	-0.21		
Cole Creek at Deihl Road	590	Brays Bayou at Bellaire Boulevard	475	0.65	0.59	0.17		
Buffalo Bayou at Dairy Ashford Road	2,290	Brays Bayou at Stella Link Road	430	Brays Bayou at South Main Street	420	0.74	0.51	0.19

Abbreviation: HCFCD, Harris County Flood Control District.

To judge whether a cell was wet or dry, a minimum threshold of 10 cm flood depth was used (Kalyanapu et al., 2011). Four evaluation metrics, including, hit rate, false alarm, critical success index, and error bias were used to quantify the difference between the modeled and derived flood inundation extents. The hit rate determines the degree in which the model was able to mimic observed wet cells, while, the false alarm quantifies the overestimation by the model (Wing et al., 2017). The critical success index statistically compares the extents by excluding the effects of dry cells. The error bias determines the tendency of the model to overestimate or underestimate the flood extent (see Wing et al. (2017) for further discussion). The comparison between the simulated maximum extent and the derived flood extent showed 78.0% hit rate, 49.3% false alarm, 44.3% critical success index, and 3.5 error bias (Figure 6). The low-density coverage of the high-water mark points in some areas has contributed to the overestimation by the model. For instance, the stage gauge station with Site-ID-1340 (Figures 5 and 6), which was one of the validation locations, has recorded a water depth value above 4.0 m during the Hurricane Harvey flood event that was not captured by the high-water mark points.

Although we have obtained good performance during the model development, the flood model in this study cannot be used for operational purpose because of two key limitations. First, the Flood2D-GPU model lacks the capability to route runoff and external inflows through stormwater drainage systems that can affect the overall mass balance. Second, the flood model also lacks the

capability to model civil and hydraulic structures such as bridges, culverts, and weirs. This can affect the accuracy of the flood depths, velocities, and flood extents around these structures. Overall, the calibration and validation results demonstrated that the Harris County flood model can be used to perform detailed sensitivity analysis.

3.2 | Sensitivity analysis

The results from the series of sensitivity analysis were used to extract simulated flood depths, relative inundation area differences, and indicative flood hazard maps (Figure 7; Table 6; Table 7) to understand the effect of each parameters on the flood model predictions. The simulated flood depths were compared at four representative sample locations. The simulated maximum flood extents were used to calculate the percentage difference in flood inundation areas, using a 10 cm flood depth as a threshold to separate dry and wet cells.

Figure 8 and Figure 9 present stage hydrographs extracted at four sample locations for selected precipitation and soil moisture condition scenarios, respectively. It is observed that both hydrologic parameters have influence on the timing, magnitude, and shape of the stage hydrographs. The peak water depths and flood inundation extents are increased by up to 2% and 6%, respectively, for a 10% increase in both hydrologic parameters (Figure 7a,b; Table 6). This result suggests that the flood model is sensitive to both precipitation and soil moisture condition and it also demonstrates that both hydrologic

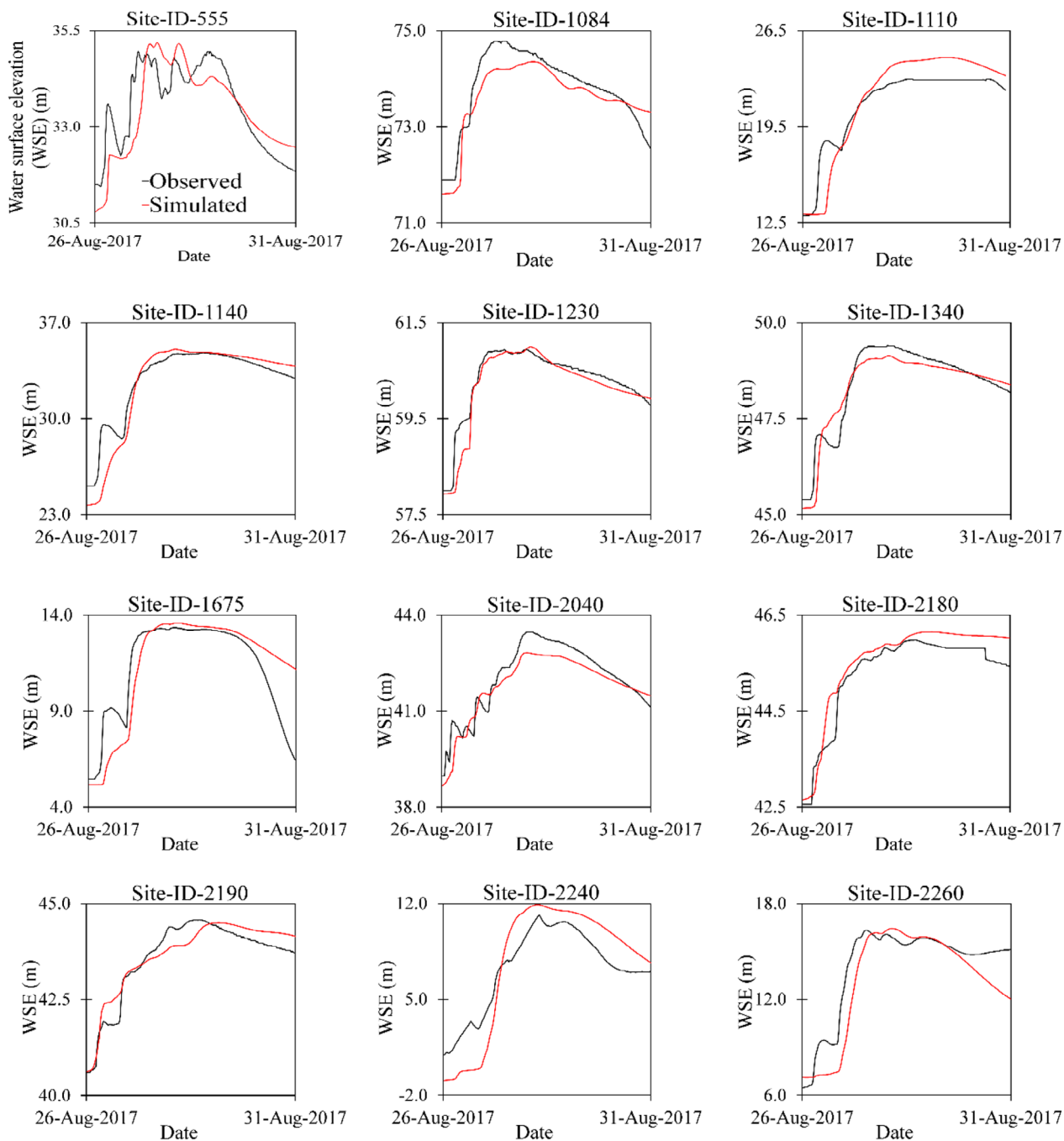


FIGURE 5 Simulated and observed water surface elevation comparison for validation of the Hurricane Harvey flood simulation. The HCFCD site IDs and site names can be found in Table 5

parameters are key factors in improving flood inundation modeling. As expected, we also found similar pattern in the flood damages where increase in the percent of precipitation and soil moisture condition increased the number of grid cells for all three flood hazard zones (Table 7). Overall, these results confirm that a high-resolution rainfall input and a good estimate of initial soil moisture condition are essential in an integrated hydrologic-hydraulic modeling framework.

Figure 10 presents simulated flood inundation depths from five scenarios with initial water depth values between 0.0 and 0.5 m. The impacts of initial water depths were significant only at the beginning of the stage hydrographs, where low flow values are dominant (Figure 10). As expected, larger initial water depth values generated higher flood inundation depths for all sample locations. However, for the selected initial water depth values, the differences in peak water depth values and

TABLE 5 Hurricane Harvey flood event validation results

Site name	HCFCD site ID	NSE	RSR	PBIAS
White Oak Bayou at Jones Road	555	0.57	0.65	0.30
Threemile Creek at Joseph Road	1,084	0.80	0.45	0.26
Cypress Creek at Cypresswood Drive	1,110	0.69	0.56	-2.34
Cypress Creek at Stuebner-Airline Road	1,140	0.80	0.45	0.50
Little Cypress Creek at Becker Road	1,230	0.87	0.36	0.19
Willow Creek at State Highway 249	1,340	0.89	0.34	0.16
Halls Bayou at Tidwell Road	1,675	0.54	0.68	-1.91
Buffalo Bayou at U.S. highway 90	2040	0.84	0.40	0.63
Bear Creek at Farm to Market Road 529	2,180	0.86	0.38	-0.55
South Mayde Creek at Peek Road	2,190	0.89	0.33	-0.16
Buffalo Bayou at Shepherd Drive	2,240	0.55	0.67	-5.91
Buffalo Bayou at San Felipe Drive	2,260	0.68	0.57	6.24

Abbreviation: HCFCD, Harris County Flood Control District.

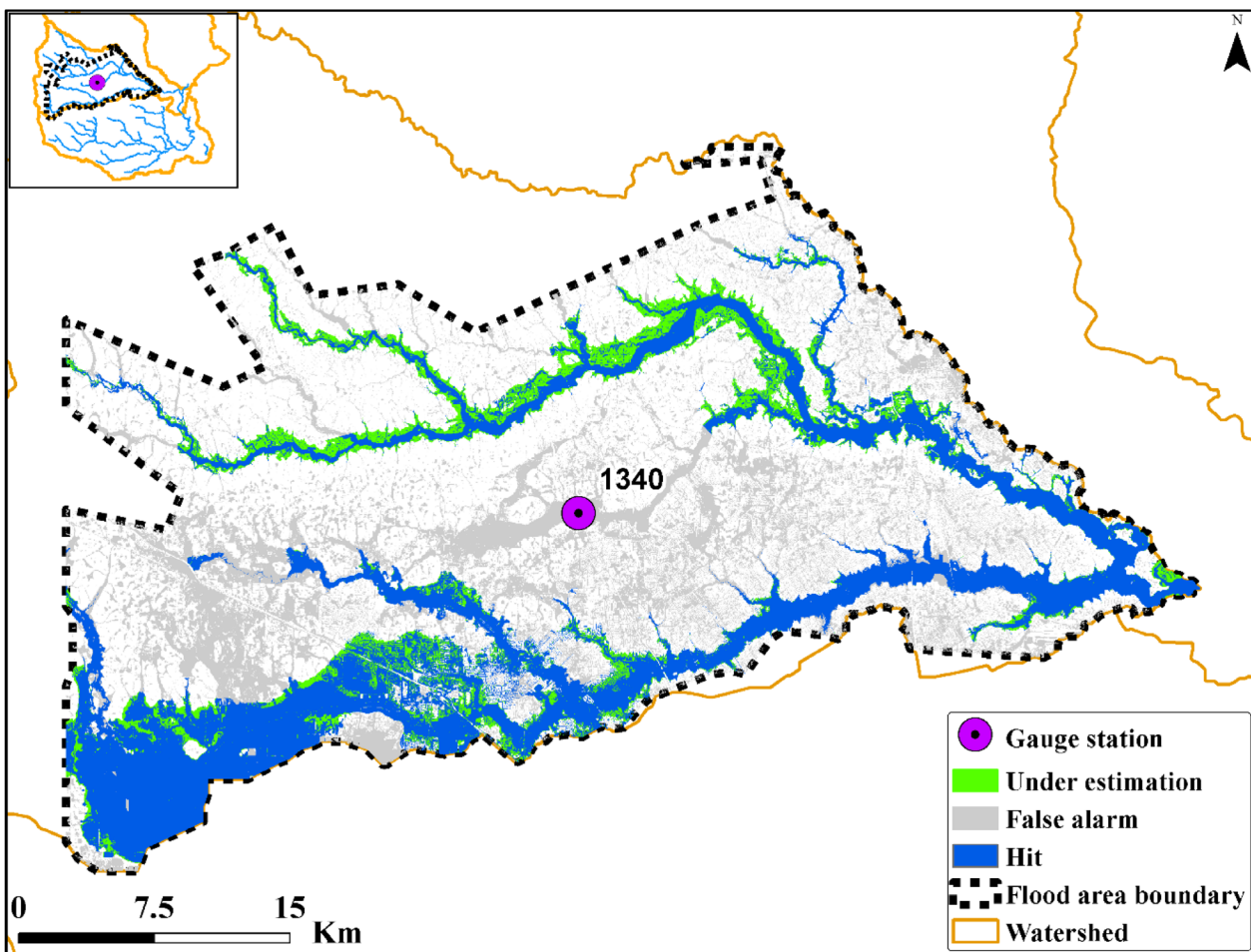


FIGURE 6 Comparison of simulated maximum flood extent with flood extent derived from observed high water mark points. The HCFCD gauge station site ID and site name can be found in Table 5

time to peak were less than 0.2% (Table 6). Although the difference in flood inundation extents relative to the 0.2 m initial water depth showed an increasing trend, the

relative differences were less than 0.02% (Table 6). Similarly, for all five scenarios, there was no clear difference (less than 0.1%) between the number of grid cells in the

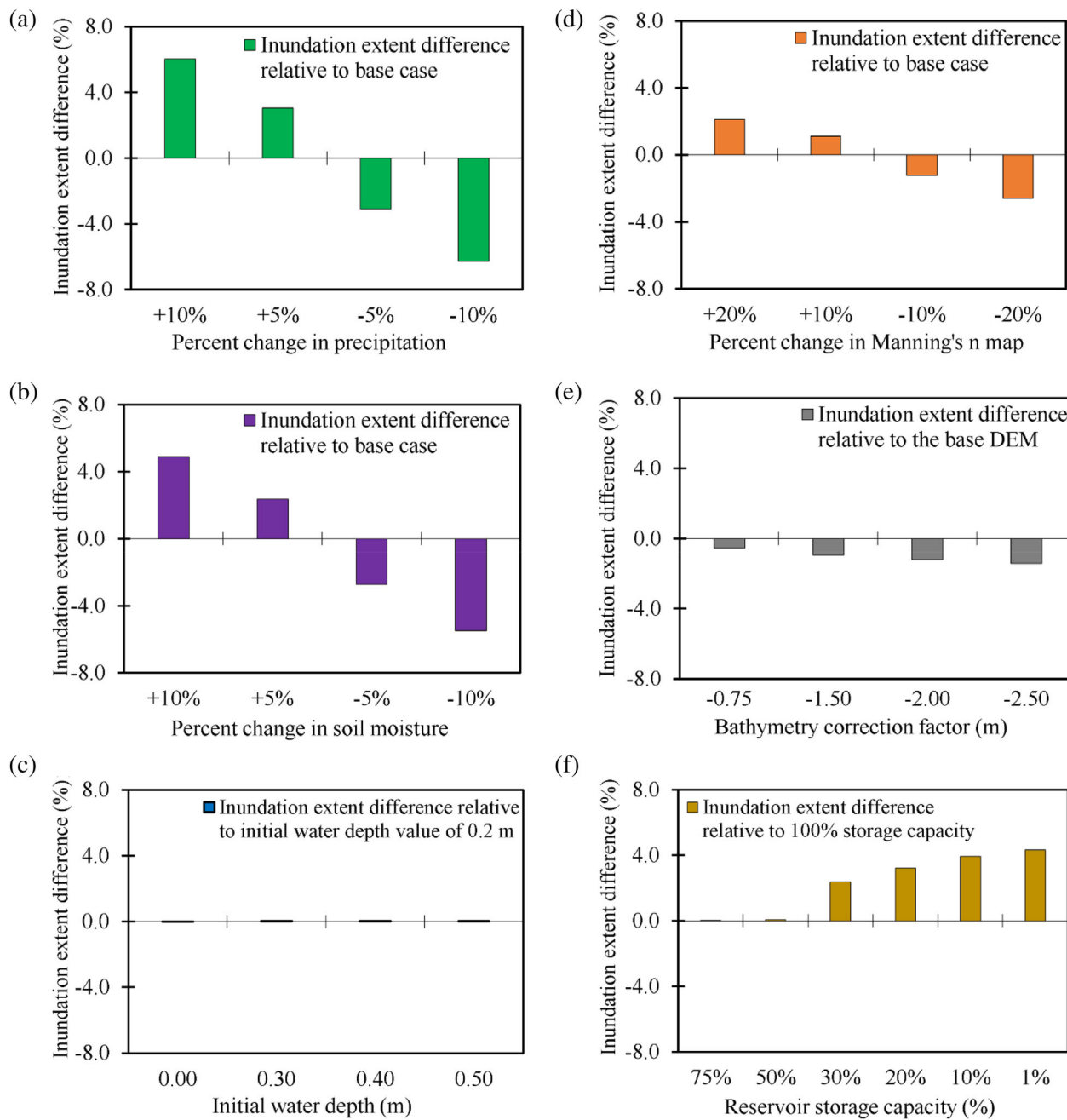


FIGURE 7 Change in simulated maximum flood extents for (a) precipitation, (b) soil moisture, (c) initial water depth, (d) Manning's *n* value, (e) bathymetry correction factor, and (f) reservoir retention capacity

low-danger zone, the judgment zone, and the high-danger zone (Table 7). Overall, for a large-magnitude flood event such as Hurricane Harvey, the impact of initial water depth on the amplitude and timing of water depth and simulated maximum flood extent was negligible.

Figure 11 summarizes simulated flood inundation depths for five different Manning's *n* value maps estimated based on NLCD 2011. The influence of the surface roughness value was significant on the peak water depths

and the falling limb of the stage hydrographs. A 20% increase in the base Manning's *n* map resulted in ~1% increase in the peak water depth value and ~2% delay in the time to peak difference (Table 6). This result indicates the sensitivity of the flood model to Manning's *n* value and the importance of surface roughness in achieving suitable representation of the magnitude and timing of the stage hydrographs. In terms of simulated maximum flood extent, the relative difference between scenario 5 (*N*_5) and the base Manning's *n* map (*N*_3) showed

TABLE 6 Change in peak water depth, time to peak, and flood inundation extent

Selected parameter	% Change in selected parameter	% Change in peak water depth	% Change in time to peak	% Change in flood inundation extent	Scenarios used to calculate the % change values
Precipitation	-10.0%	-2.63	2.31	-6.29	Base case (P_3)
	-5.0%	-1.27	1.59	-3.09	
	0.0%	0.00	0.00	0.00	
	5.0%	1.20	-0.39	3.04	
	10.0%	2.26	-5.89	6.02	
Soil moisture	-10.0%	-2.38	7.08	-5.49	Base case (SM_3)
	-5.0%	-1.14	2.08	-2.73	
	0.0%	0.00	0.00	0.00	
	5.0%	1.01	-0.39	2.37	
	10.0%	2.28	-5.60	4.89	
Initial water depth	-100.0%	-0.03	0.00	-0.02	0.20 m water depth
	0.0%	0.00	0.00	0.00	
	50.0%	0.01	0.00	0.01	
	100.0%	0.02	-0.13	0.01	
	150.0%	0.03	-0.13	0.02	
Manning's <i>n</i> value	-20.00%	-1.32	-2.20	-2.60	Manning's <i>n</i> value base map (N_3)
	-10.00%	-0.62	-1.67	-1.23	
	0.00%	0.00	0.00	0.00	
	10.00%	0.54	0.96	1.10	
	20.00%	1.00	1.54	2.11	
Bathymetry correction factor	-100.00%	-12.79	-0.13	0.96	Bathymetry correction factor of -1.5 m
	-50.00%	-6.40	-0.13	0.43	
	0.00%	0.00	0.00	0.00	
	33.33%	4.27	0.52	-0.26	
	66.67%	8.56	0.81	-0.49	
Reservoir storage capacity	100%	0.00	0.00	0.00	100% storage capacity
	75%	0.00	0.00	0.00	
	50%	0.03	0.00	0.05	
	30%	20.18	79.26	2.36	
	20%	24.43	65.57	3.21	
	10%	27.64	50.55	3.93	
	1%	28.82	31.74	4.31	

~2% (65 km²) change in inundation area (Figure 7d; Table 6). The percent change in the number of grid cells for the three flood hazard zones showed an increasing trend with increasing surface roughness values. A 20% increase in the base Manning's *n* value map shows increases of approximately 1, 5, and 7% in the number of cells corresponding to the low-danger, judgment, and high-danger zone, respectively (Table 7). These results demonstrate that the Flood2D-GPU is more sensitive to surface roughness values than initial water depths, which

makes the Manning's *n* value an essential hydraulic parameter in the calibration and validation of large-scale and high-resolution flood inundation modeling.

The four insets in Figure 12 illustrate the flood inundation depths for five scenarios with bathymetry correction factors ranging from 0.0 m to -2.5 m. For all sample locations, higher bathymetry correction factors result in larger peak depths and higher water depths in the recession limb of the stage hydrographs (Figure 12). A 67% increase in the bathymetry correction factor increased

Selected parameter	% Change in selected parameter	% Change in area			Scenarios used to calculate the % change values
		Low danger zone	Judgment zone	High danger zone	
Precipitation	-10.0%	-4.02	-12.10	-14.14	Base case (P_3)
	-5.0%	-1.83	-6.42	-7.34	
	0.0%	0.00	0.00	0.00	
	5.0%	1.68	6.67	7.57	
	10.0%	3.24	13.30	15.47	
Soil moisture	-10.0%	-2.46	-14.38	-14.85	Base case (SM_3)
	-5.0%	-1.23	-6.99	-7.47	
	0.0%	0.00	0.00	0.00	
	5.0%	1.17	5.50	6.50	
	10.0%	2.41	11.42	13.29	
Initial water depth	-100.0%	-0.01	-0.02	-0.08	0.20 m water depth
	0.0%	0.00	0.00	0.00	
	50.0%	0.00	0.01	0.03	
	100.0%	0.00	0.02	0.05	
	150.0%	0.01	0.02	0.09	
Manning's <i>n</i> value	-20.00%	-1.06	-7.61	-6.56	Manning's <i>n</i> value base map (N_3)
	-10.00%	-0.51	-3.31	-3.35	
	0.00%	0.00	0.00	0.00	
	10.00%	0.46	2.61	3.38	
	20.00%	0.85	5.16	6.52	
Bathymetry correction factor	-100.00%	0.24	2.22	4.07	Bathymetry correction factor of - 1.5 m
	-50.00%	0.10	0.95	1.96	
	0.00%	0.00	0.00	0.00	
	33.33%	-0.06	-0.41	-1.32	
	66.67%	-0.11	-0.68	-2.66	
Reservoir storage capacity	100%	0.00	0.00	0.00	100% storage capacity
	75%	0.01	-0.02	0.00	
	50%	0.02	0.08	0.30	
	30%	1.43	10.49	4.30	
	20%	1.45	18.11	7.08	
	10%	0.91	24.92	13.50	
	1%	0.78	26.31	17.24	

TABLE 7 Change of flood hazard zone classification

the peak water depth and time to peak by ~9% and ~1%, respectively (Table 6). This result indicates that inaccurate representation of river bathymetry can have significant impact on the magnitude and timing of the stage hydrograph. The simulated maximum flood extents show a continuous decrease as the bathymetry correction factor is increased, with inundation extent differences ranging from around 0.5 to 1.4% (Figure 7e). This is because increasing the bathymetry correction factor increased the

volume of the channel, thereby allowing a large portion of the flow to be conveyed through the main channel instead of spreading onto the floodplain areas. The result confirms that the inability to capture the river bathymetry accurately may lead to large deviation in the estimated flood extent. As expected, the percent change in the number of grid cells in each flood hazard category shows a continuous decrease as the bathymetry correction factors increase. Compared with the -1.5 m

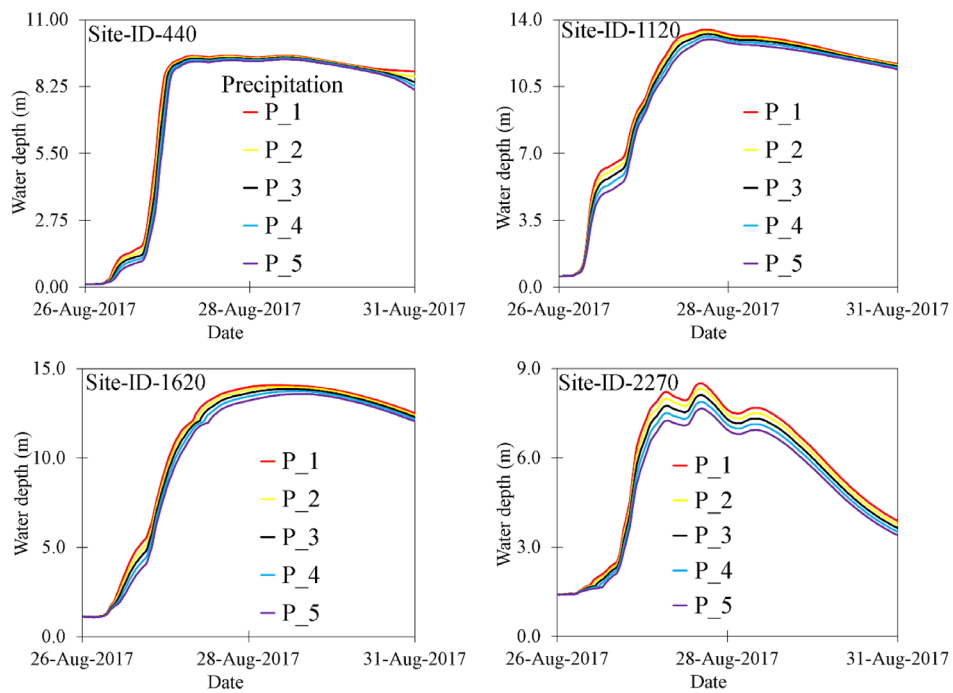


FIGURE 8 Simulated flood depths for selected precipitation values. The gauge locations are shown in Figure 1. Descriptions for precipitation values are presented in Table 1

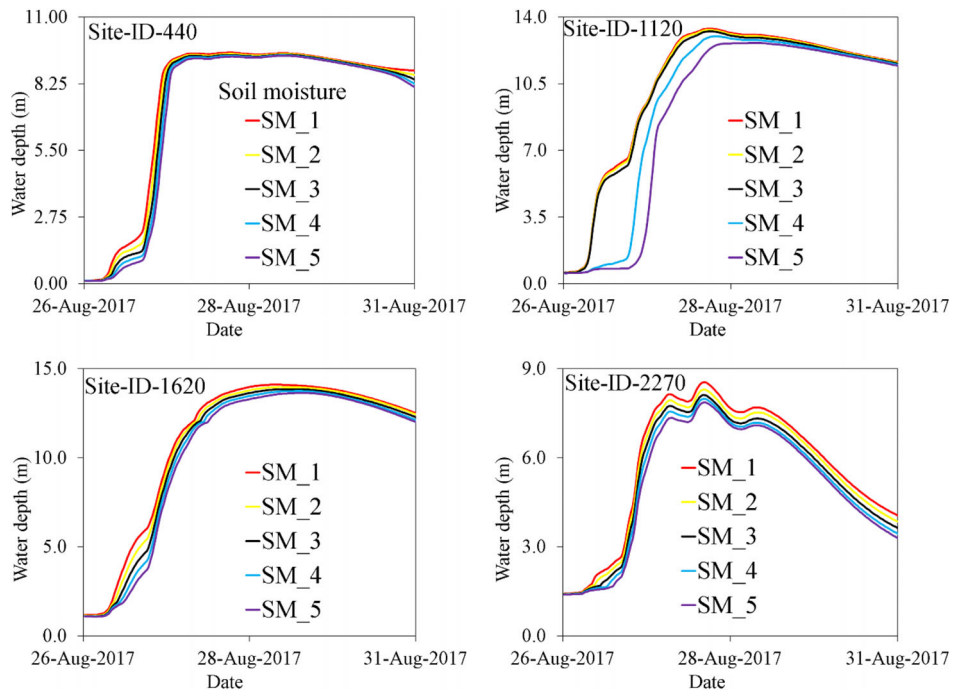


FIGURE 9 Simulated flood depths for selected soil moisture values. The gauge locations are shown in Figure 1. Descriptions for soil moisture conditions are presented in Table 1

correction factor, the use of base DEM increases the percent change in the number of cells for the low-danger, judgment, and high-danger zones by up to 0.2, 2.2, and

4.0%, respectively (Table 7). The percentage decrease in the number of grid cells indicates that the error in the base DEM can result in a false flag for floodplain managers

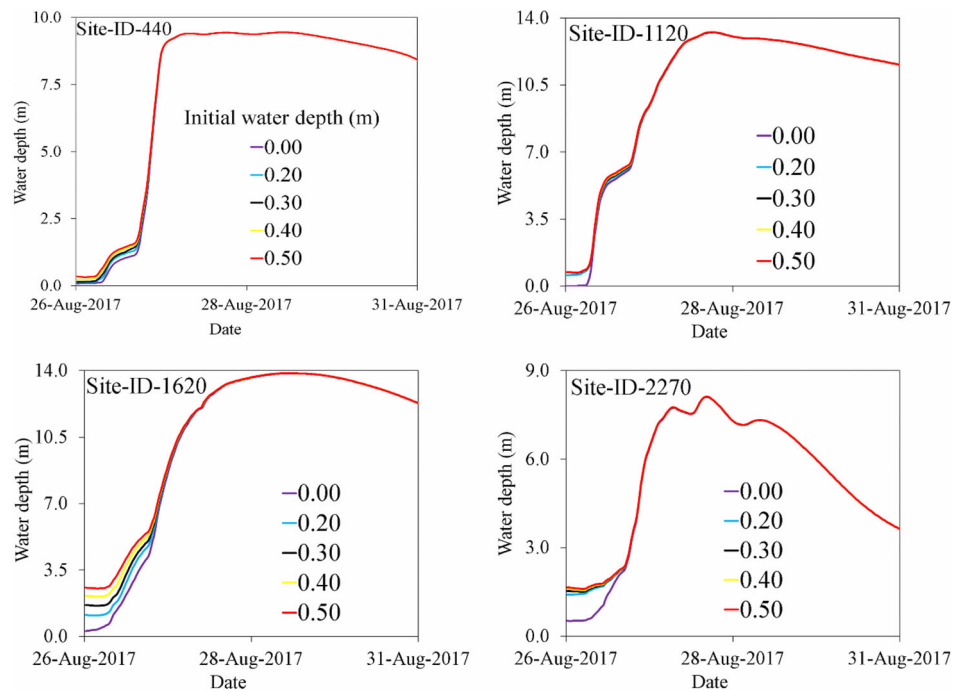


FIGURE 10 Simulated flood depths for selected initial water depth values. The gauge locations are shown in Figure 1

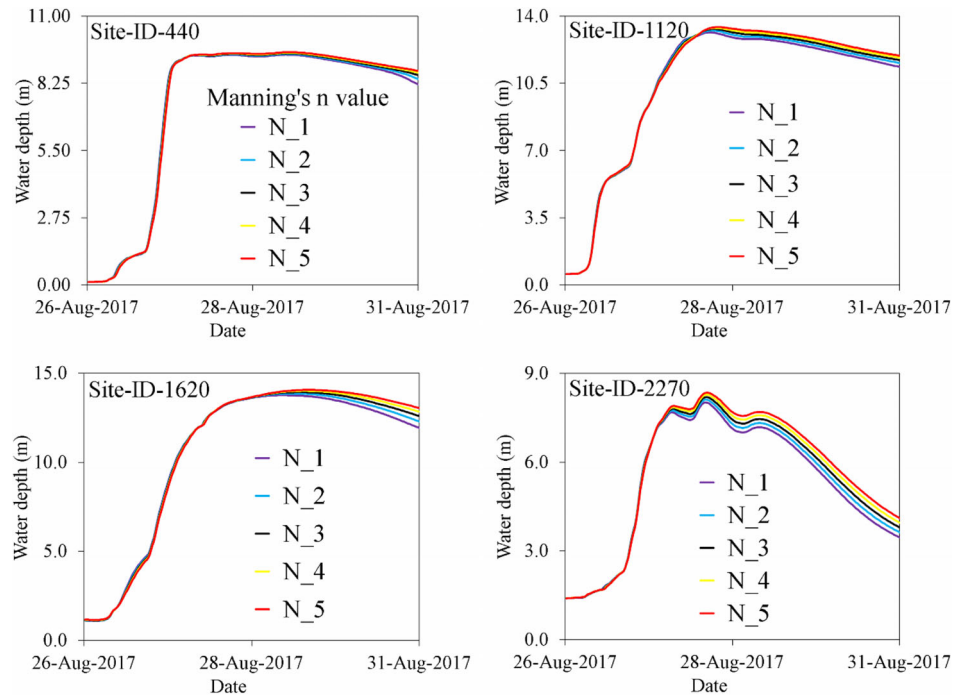


FIGURE 11 Simulated flood depths for selected Manning's n values. The gauge locations are shown in Figure 1. Descriptions for Manning's n values are presented in Table 1

developing flood hazard zones using raw DEM products. Overall, the results demonstrated the importance of improving the quality of base DEM and the relative sensitivity of the flood model to the bathymetry error.

Based on the reservoir storage capacity, the flood depths, relative inundation areas, and flood hazard maps were summarized only for the area downstream of the two reservoirs. The watershed boundaries obtained from

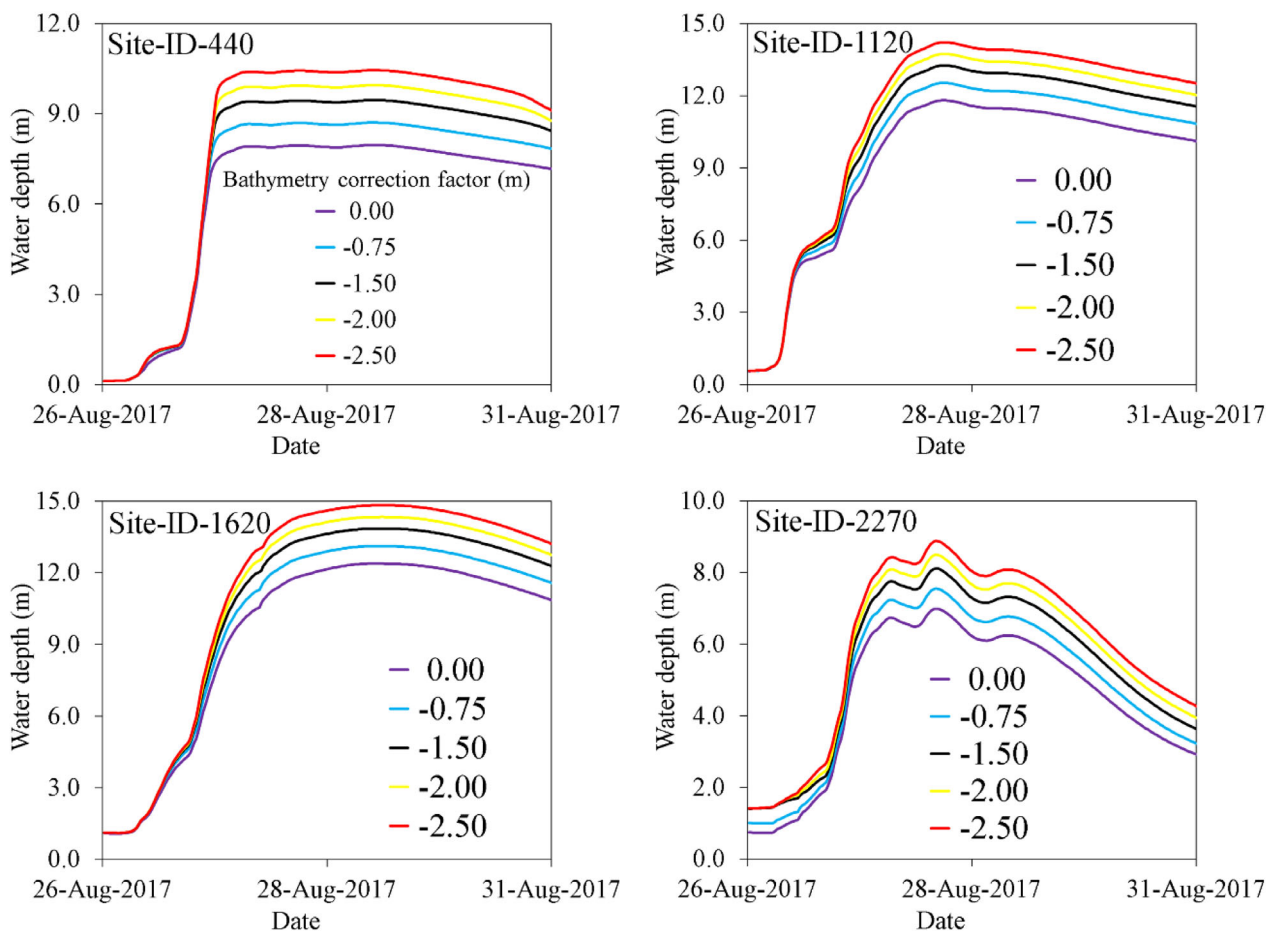


FIGURE 12 Simulated flood depths for selected bathymetry correction factors. The gauge locations are shown in Figure 1

HCFCD (HCFCD, 2019) were used to prepare the areas downstream of the two reservoirs. Figure 13 presents the flood inundation depths extracted at four sample locations. In all sample locations, for scenarios below 30% storage capacity, there is a significant change in the magnitude and shape of the stage hydrographs. Reducing the storage capacity to 1%, increased the peak water depth value by up to 28% and the time to peak by up to 31% (Table 6). The effects of reservoir storage capacity on downstream flooding are further illustrated in Table 6 and Figure 14. For scenarios below 30% storage, the flood inundation extent downstream of the reservoirs increases as the storage capacity is reduced (Figure 7f; Table 6). Storage cases above 50% do not show significant differences from the 100% storage case, suggesting that during Hurricane Harvey, both reservoirs could have sufficiently held the reservoir inflow, even for storage capacities as low as 50%. This result may initially seem counter-intuitive, considering the large flood that occurred in the downstream Houston areas. However, it can be explained by the fact that a majority of the heaviest Hurricane Harvey rainfall occurred downstream of the reservoirs, so the flood impacts could not be fully reduced through

regulation. From a modeling perspective, the results shown in Figure 14b-f suggest that reservoir storage can greatly impact flooding results, so there is a need to address its effect on large-scale flood simulation through further reservoir regulation model coupling. The results of Figure 14a further suggest the event-specific nature of flood simulation. The location, movement, and structure of extreme storm events can result in complicated flood responses that can hardly be generalized. As expected, both Table 7 and Figure 15 show increases in the three flood hazard categories as storage capacity is reduced. Compared with full storage capacity, the 1% storage case (Figure 15f) results in grid cells that are classified as being at higher risk for the low-danger, judgment, and high-danger zones by up to 1, 26, and 17%, respectively. The percentage increase in flood risks demonstrates the importance of incorporating reservoir operation and regulation in developing flood hazard maps. With the advances occurring in rainfall forecasting resolution and accuracy, large-scale, high-resolution and coupled hydrologic-hydraulic modeling capacity will be needed to adequately simulate the corresponding flood response.

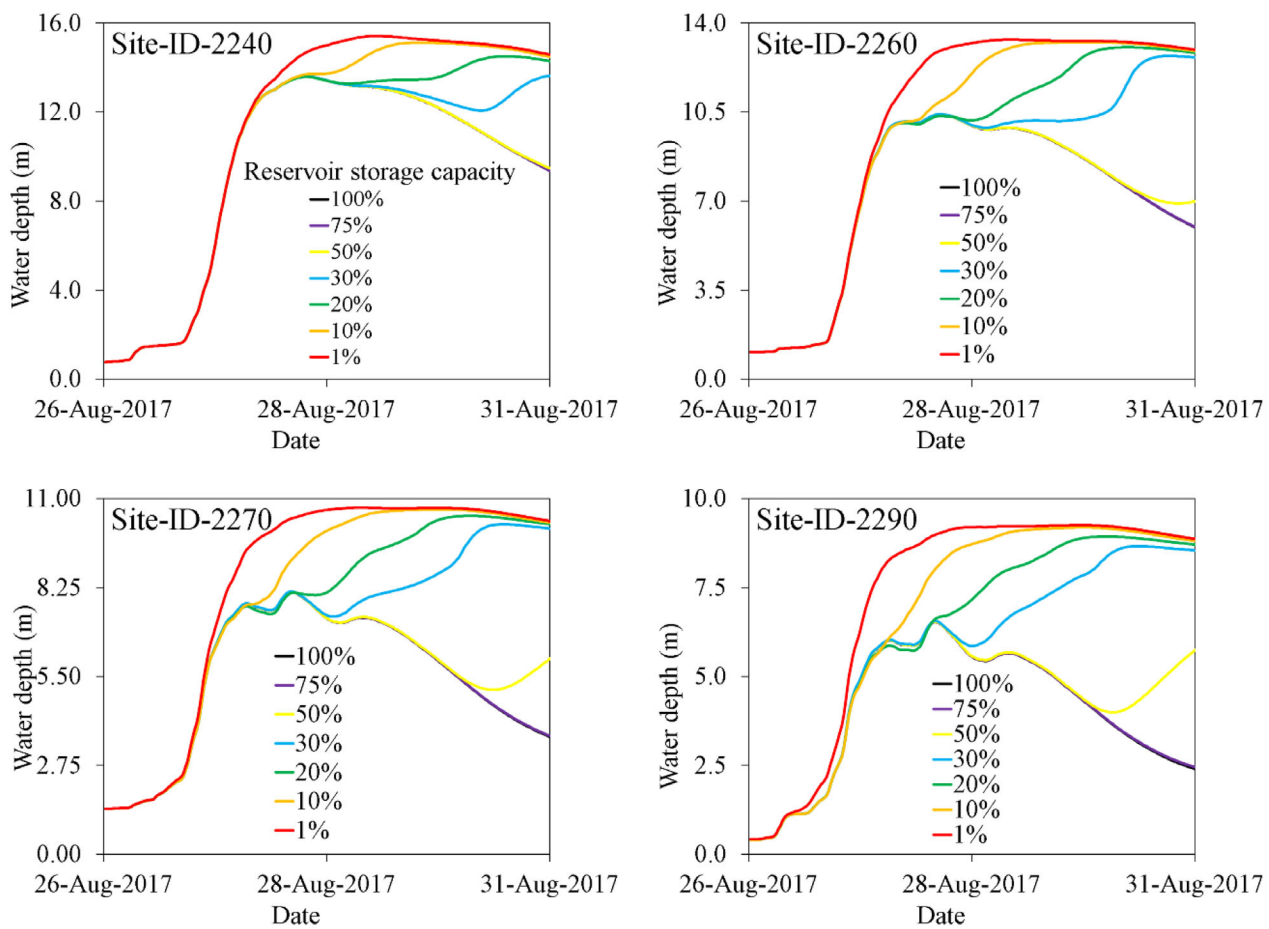


FIGURE 13 Simulated flood depths for selected reservoir storage capacities. The gauge locations are shown in Figure 1

4 | SUMMARY

This paper highlights three challenges associated with large-scale coupled hydrologic-hydraulic modeling simulations. They include (a) model parameterization, (b) errors in digital elevation models, and (c) effects of reservoir retention. The coupled modeling framework was performed by setting up a series of sensitivity analyses to quantify and compare their respective influence using Hurricane Harvey as a test case. Radar-based hourly ST4 rainfall data were used to drive the VIC model for all four HUC08 watersheds in the San Jacinto River Basin. The simulated hourly VIC total runoff was then routed using the RAPID model through the NHD+ river network to simulate streamflow along the boundary of the computation domain. The hourly runoff and streamflow hydrographs from VIC and RAPID, respectively, were then used to derive the Flood2D-GPU model that was set up over Harris County, Texas. After model evaluation, the flood inundation responses associated with different hydrologic and hydraulic model parameterizations, bathymetry correction factors (i.e., errors in digital

elevation models), and reservoir storage capacities were evaluated to understand their relative importance in a large-scale flood simulation.

The results suggest that both precipitation and soil moisture condition have influence on the timing, magnitude, and shape of the stage hydrographs. The peak water depths and flood inundation extents are increased by up to 2% and 6%, respectively, for a 10% increase in the hydrologic parameters. For the hydraulic parameters, the effects of initial water depths were significant only at the beginning of the flood event when low flow values were dominant. There were no significant differences in flood inundation extents and flood hazards for all five initial water depth scenarios. However, a 20% increase in the base Manning's n map resulted in ~1% increase in the peak water depth value, ~2% delay in the time to peak difference, and ~2% (65 km^2) increase in the inundation area. Similarly, a 20% increase in surface roughness values increased the flood risks for the low-danger, judgment, and high-danger zones by around 1, 5, and 6%, respectively. On the contrary, increasing the bathymetry correction factor to -2.5 m reduced the flood inundation

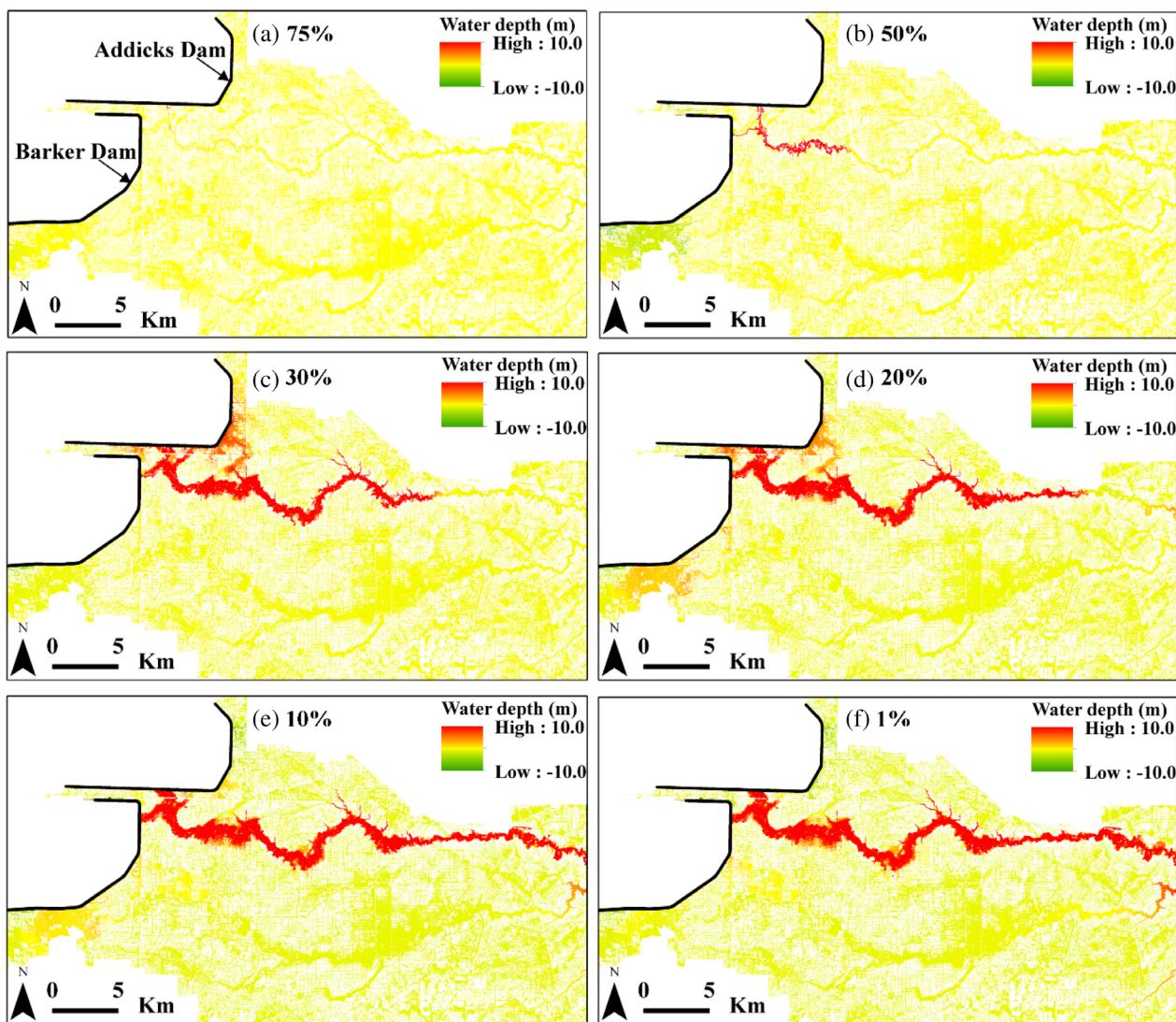


FIGURE 14 Change in simulated maximum flood inundation depths relative to full storage capacity for (a) 75%, (b) 50%, (c) 30%, (d) 20%, (e) 10%, and (f) 1% storages

extent by up to 1.4% and reduced the high-danger zone by up to 4%. Reducing the storage capacity to 1%, increased the peak water depth values and flood inundation extents downstream of the reservoirs by up to 28 and 4%, respectively. Compared with full storage capacity, the 1% storage case had grid cells that were classified at higher risk for the low-danger, judgment, and high-danger zones by up to 1, 26, and 17%, respectively.

In summary, since the flood model is sensitive to the hydrologic parameters, a high-resolution rainfall input and a good estimate of initial soil moisture condition are essential in an integrated hydrologic-hydraulic modeling framework. For a large-magnitude flood event such as Hurricane Harvey, the impact of initial water depths on the simulated maximum flood extent was negligible. However, the high sensitivity of the Flood2D-GPU to

surface roughness indicates that the Manning's n value is an essential hydraulic parameter in the calibration and validation of large-scale, high-resolution flood inundation modeling. For the bathymetry correction factor, the change in flood depths and flood inundation extents indicates that flood modelers need to improve the accuracy of the base DEM during the calibration and validation process. In addition, the error in the base DEM can result in a false flag for floodplain managers developing flood hazard zones using raw DEM products. For the reservoir storage capacity, the percentage increases in flood depth, flood extent, and flood risk downstream of the two reservoirs demonstrate the importance of incorporating reservoir operation and regulation in large-scale flood simulation. The broader implications of this study will be useful in flood risk management, as it provides additional information on the effects of the selected sensitivity

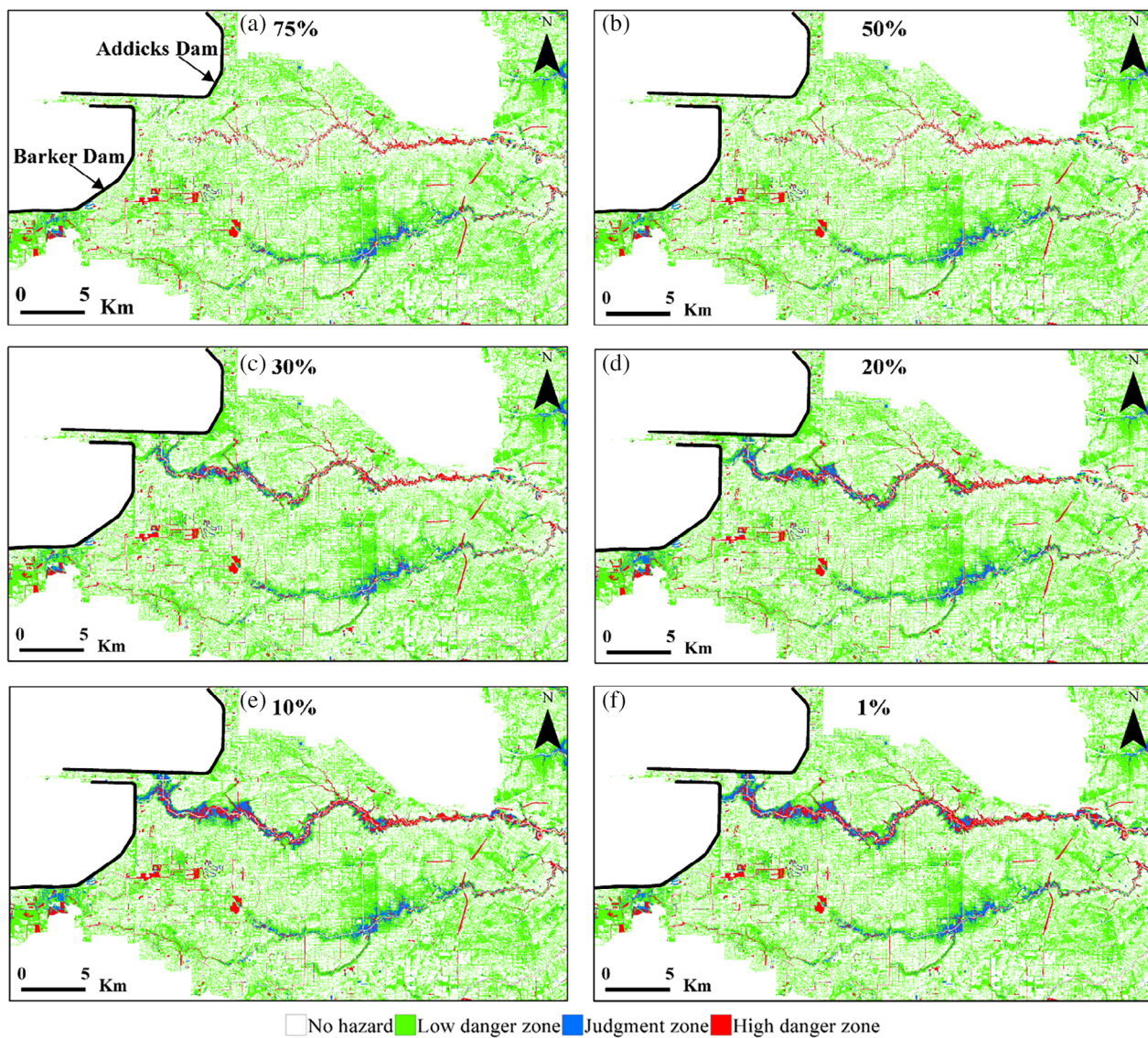


FIGURE 15 Flood risk maps for (a) 75%, (b) 50%, (c) 30%, (d) 20%, (e) 10%, and (f) 1% storages

parameters in the calibration of large-scale flood simulation and their corresponding impacts on flood damage estimates.

ACKNOWLEDGEMENTS

This study was supported by the US Air Force Numerical Weather Modeling Program. The research used resources of the Oak Ridge Leadership Computing Facility at Oak Ridge National Laboratory. The authors also acknowledge support by the Center of Management, Utilization, and Protection of Water Resources at Tennessee Technological University. Some of the co-authors are employees of UT-Battelle LLC under contract DE-AC05-00OR22725 with the US Department of Energy. Accordingly, the US government retains and the publisher, by accepting the article for publication, acknowledges that the US government retains a nonexclusive,

paid-up, irrevocable, worldwide license to publish or reproduce the published form of this manuscript, or allow others to do so, for US Government purposes. The input data sets are cited throughout the paper, as appropriate.

DATA AVAILABILITY STATEMENT

The data that support the findings of this study are openly available in figshare repository at the following URL: <https://doi.org/10.6084/m9.figshare.12509846>.

ORCID

Sudershan Gangrade  <https://orcid.org/0000-0002-0730-0810>

Shih-Chieh Kao  <https://orcid.org/0000-0002-3207-5328>

Alfred J. Kalyanapu  <https://orcid.org/0000-0002-7746-3121>

REFERENCES

- ACER Technical Memorandum No. 11. (1988). *Assistant commissioner—Engineering and research, downstream hazard classification guidelines*. Denver, Colorado: U.S. Department of the Interior, Bureau of Reclamation.
- Annis, A., Nardi, F., Morrison, R. R., & Castelli, F. (2019). Investigating hydrogeomorphic floodplain mapping performance with varying DTM resolution and stream order. *Hydrological Sciences Journal*, 64(5), 525–538. <https://doi.org/10.1080/02626667.2019.1591623>
- Archuleta, C.-A. M., Constance, E. W., Arundel, S. T., Lowe, A. J., Mantey, K. S., & Phillips, L. A. (2017). The National Map Seamless Digital Elevation Model Specifications, U.S. Geological Survey Techniques and Methods 11-B9. <https://pubs.er.usgs.gov/publication/tm11B9>.
- Aronica, G., Bates, P. D., & Horritt, M. S. (2002). Assessing the uncertainty in distributed model predictions using observed binary pattern information within GLUE. *Hydrological Processes*, 16(10), 2001–2016. <https://doi.org/10.1002/hyp.398>
- Bass, D., O'Connor, B., & Perotin, M. (2018). A summary of Findings from FEMA's mitigation assessment team evaluation of Texas coastal communities impacted by Hurricane Harvey. *Forensic Engineering*, 2018, 833–845. <https://doi.org/10.1061/9780784482018.081>
- Bates, P. D., Horritt, M. S., & Fewtrell, T. J. (2010). A simple inertial formulation of the shallow water equations for efficient two dimensional flood inundation modelling. *Journal of Hydrology*, 387, 33–45. <https://doi.org/10.1016/j.jhydrol.2010.03.027>
- Baugh, C. A., Bates, P. D., Schumann, G., & Trigg, M. A. (2013). SRTM vegetation removal and hydrodynamic modeling accuracy. *Water Resources Research*, 49, 5276–5289. <https://doi.org/10.1002/wrcr.20412>
- Bhuyian, M. N. M., Kalyanapu, A. J., & Nardi, F. (2014). Approach to digital elevation model correction by improving channel conveyance. *Journal of Hydrologic Engineering*, 20(5), 4014062. [https://doi.org/10.1061/\(ASCE\)HE.1943-5584.0001020](https://doi.org/10.1061/(ASCE)HE.1943-5584.0001020)
- Brakebill, J. W., Wolock, D. M., & Terziotti, S. E. (2011). Digital hydrologic networks supporting applications related to spatially referenced regression modeling. *Journal of American Water Resources Association*, 47(5), 916–932. <https://doi.org/10.1111/j.1752-1688.2011.00578.x>
- Casas, A., Benito, G., Thorndycraft, V. R., & Rico, M. (2006). The topographic data source of digital terrain models as a key element in the accuracy of hydraulic flood modeling. *Earth Surface Processes and Landforms*, 31(4), 444–456. <https://doi.org/10.1002/esp.1278>
- Cea, L., & French, J. R. (2012). Bathymetric error estimation for the calibration and validation of estuarine hydrodynamic models. *Estuarine, Coastal and Shelf Science*, 100, 124–132. <https://doi.org/10.1016/j.ecss.2012.01.004>
- Conner, J. T., & Tonina, D. (2014). Effect of cross-section interpolated bathymetry on 2D hydrodynamic model results in a large river. *Earth Surface Processes and Landforms*, 39(4), 463–475. <https://doi.org/10.1002/esp.3458>
- Cook, A., & Merwade, V. (2009). Effect of topographic data, geometric configuration and modeling approach on flood inundation mapping. *Journal of Hydrology*, 377(1–2), 131–142. <https://doi.org/10.1016/j.jhydrol.2009.08.015>
- da Silva, J. C. B., Buijsman, M. C., & Magalhaes, J. M. (2015). Internal waves on the upstream side of a large sill of the Mascarene ridge: A comprehensive view of their generation mechanisms and evolution. *Deep-Sea Research I*, 99, 87–104. <https://doi.org/10.1016/j.dsr.2015.01.002>
- da Silva, M. G., de Aguiar Netto, A., de Jesus Neves, R., do Vasco, A. N., Almeida, C., & Faccioli, G. G. (2015). Sensitivity analysis and calibration of hydrological modeling of the watershed Northeast Brazil. *Journal of Environmental Protection*, 6(8), 837–850. <https://doi.org/10.4236/jep.2015.68076>
- Daly, C., Halbleib, M., Smith, J. I., Gibson, W. P., Doggett, M. K., Taylor, G. H., ... Pasteris, P. P. (2008). Physiographically sensitive mapping of climatological temperature and precipitation across the conterminous United States. *International Journal of Climatology*, 28(15), 2031–2064. <https://doi.org/10.1002/joc.1688>
- Dung, N. V., Merz, B., Bárdossy, A., Thang, T. D., & Apel, H. (2011). Multi-objective automatic calibration of hydrodynamic models utilizing inundation maps and gauge data. *Hydrology and Earth System Sciences*, 15, 1339–1354. <https://doi.org/10.5194/hess-15-1339-2011>
- Emerton, R. E., Stephens, E. M., Pappenberger, F., Pagano, T., C., Weerts, A. H., Wood, A. W., ... Cloke, H. L. (2016). Continental and global scale flood forecasting systems. *Wiley Interdisciplinary Reviews (WIREs) Water*, 3, 391–418. <https://doi.org/10.1002/wat2.1137>
- Fleischmann, A., Collischonn, W., Paiva, R., & Tucci, C. E. (2019). Modeling the role of reservoirs versus floodplains on large-scale river hydrodynamics. *Natural Hazards*, 99(2), 1075–1104. <https://doi.org/10.1007/s11069-019-03797-9>
- Forbes, W. L., Mao, J., Ricciuto, D. M., Kao, S.-C., Shi, X., Tavakoly, A. A., ... Hoffman, F. M. (2019). Streamflow in the Columbia River basin: Quantifying changes over the period 1951–2008 and determining the drivers of those changes. *Water Resources Research*, in press, 55, 6640–6652. <https://doi.org/10.1029/2018WR024256>
- Gangrade, S., Kao, S.-C., Dullo, T. T., Kalyanapu, A. J., & Preston, B. L. (2019). Ensemble-based flood vulnerability assessment for probable maximum flood in a changing environment. *Journal of Hydrology*, 576, 342–355. <https://doi.org/10.1016/j.jhydrol.2019.06.027>
- Getirana, A., Peters-Lidard, C., Rodell, M., & Bates, P. D. (2017). Trade-off between cost and accuracy in large-scale surface water dynamic modeling. *Water Resources Research*, 53(6), 4942–4955. <https://doi.org/10.1002/2017WR020519>
- Gourley, J. J., Hong, Y., Flamig, Z. L., Li, L., & Wang, J. (2010). Intercomparison of rainfall estimates from radar, satellite, gauge, and combinations for a season of record rainfall. *Journal of Applied Meteorology and Climatology*, 49, 437–452. <https://doi.org/10.1175/2009JAMC2302.1>
- Grimaldi, S., Schumann, G. J.-P., Shokri, A., Walker, J. P., & Pauwels, V. R. N. (2019). Challenges, opportunities and pitfalls for global coupled hydrologic-hydraulic modeling of floods. *Water Resources Research*, 55, 5277–5300. <https://doi.org/10.1029/2018WR024289>
- HCFCD (Harris County Flood Control District). (2016). *Capital Improvement Program Annual Review*. https://www.hcfcd.org/media/1997/cip_report_fy2017_final_no_project_sheets.pdf.

- HCFCD (Harris County Flood Control District). (2018). Hurricane Harvey—Storm and Flood Information. <https://www.hcfcd.org/media/2678/immediate-flood-report-final-hurricane-harvey-2017.pdf>.
- HCFCD (Harris County Flood Control District). (2019). Harris County Watersheds and Channels Reference Guide. <https://www.hcfcd.org/media/1575/watershedschannelsreferenceguide07.pdf>.
- Horritt, M. S. (2006). A linearized approach to flow resistance uncertainty in a 2-D finite volume model of flood flow. *Journal of Hydrology*, 316(1–4), 13–27. <https://doi.org/10.1016/j.jhydrol.2005.04.009>
- Kalyanapu, A. J., Burian, S. J., & McPherson, T. N. (2010). Effect of land use-based surface roughness on hydrologic model output. *Journal of Spatial Hydrology*, 9(2), 51–71.
- Kalyanapu, A. J., Judi, D. R., McPherson, T. N., & Burian, S. J. (2012). Monte Carlo-based flood modelling framework for estimating probability weighted flood risk. *Journal of Flood Risk Management*, 5(1), 37–48. <https://doi.org/10.1111/j.1753-318X.2011.01123.x>
- Kalyanapu, A. J., Shankar, S., Pardyjak, E. R., Judi, D. R., & Burian, S. J. (2011). Assessment of GPU computational enhancement to a 2D flood model. *Environmental Modelling and Software*, 26(8), 1009–1016. <https://doi.org/10.1016/j.envsoft.2011.02.014>
- Kao, S.-C., DeNeale, S. T., & Watson, D. B. (2019). Hurricane Harvey highlights: Need to assess the adequacy of probable maximum precipitation estimation methods. *Journal of Hydrologic Engineering*, 24(4), 05019005. [https://doi.org/10.1061/\(ASCE\)HE.1943-5584.0001768](https://doi.org/10.1061/(ASCE)HE.1943-5584.0001768)
- Liang, X., Lettenmaier, D. P., Wood, E. F., & Burges, S. J. (1994). A simple hydrologically based model of land surface water and energy fluxes for general circulation models. *Journal of Geophysical Research*, 99(D7), 14415–14428. <https://doi.org/10.1029/94JD00483>
- Lim, N. J., & Brandt, S. A. (2019). Flood map boundary sensitivity due to combined effects of DEM resolution and roughness in relation to model performance. *Geomatics, Natural Hazards and Risk*, 10(1), 1613–1647. <https://doi.org/10.1080/19475705.2019.1604573>
- Lin, Y. (2011). GCIP/EOP Surface: Precipitation NCEP/EMC 4KM Gridded Data (GRIB) Stage IV Data, Version 1.0, UCAR/NCAR—Earth Observing Laboratory. <http://data.eol.ucar.edu/dataset/21.093>.
- Liu, Y. Y., Maidment, D. R., Tarboton, D. G., Zheng, X., & Wang, S. (2018). A CyberGIS integration and computation framework for high-resolution continental-scale flood inundation mapping. *Journal of American Water Resources Association*, 54(4), 770–784. <https://doi.org/10.1111/1752-1688.12660>
- Luitel, B., Villarini, G., & Vecchi, G. A. (2018). Verification of the skill of numerical weather prediction models in forecasting rainfall from U.S. Landfalling tropical cyclones. *Journal of Hydrology*, 556, 1026–1037. <https://doi.org/10.1016/j.jhydrol.2016.09.019>
- Manfreda, S., Nardi, F., Samela, C., Grimaldi, S., Taramasso, A. C., Roth, G., & Sole, A. (2014). Investigation on the use of geomorphic approaches for the delineation of flood prone areas. *Journal of Hydrology*, 517, 863–876. <https://doi.org/10.1016/j.jhydrol.2014.06.009>
- Massari, C., Brocca, L., Barbetta, S., Papathanasiou, C., Mimikou, M., & Moramarco, T. (2014). Using globally available soil moisture indicators for flood modelling in Mediterranean catchments. *Hydrology and Earth System Sciences*, 18(2), 839–853. <https://doi.org/10.5194/hess-18-839-2014>
- Massari, C., Brocca, L., Moramarco, T., Tramblay, Y., & Didon Lescot, J.-F. (2014). Potential of soil moisture observations in flood modelling: Estimating initial conditions and correcting rainfall. *Advances in Water Resources*, 74, 44–53. <https://doi.org/10.1016/j.advwatres.2014.08.004>
- Mateo, C. M., Hanasaki, N., Komori, D., Tanaka, K., Kiguchi, M., Champathong, A., ... Oki, T. (2014). Assessing the impacts of reservoir operation to floodplain inundation by combining hydrological, reservoir management, and hydrodynamic models. *Water Resources Research*, 50, 7245–7266. <https://doi.org/10.1002/2013WR014845>
- McKay, L., Bondelid, T., Dewald, T., Johnston, J., Moore, R., & Rea, A. (2012). NHDPlus Version 2: User Guide. ftp://ftp.horizon-systems.com/NHDplus/NHDPlusV21/Documentation/NHDPlusV2_User_Guide.pdf.
- McKean, J., Tonina, D., Bohn, C., & Wright, C. W. (2014). Effects of bathymetric lidar errors on flow properties predicted with a multidimensional hydraulic model. *Journal of Geophysical Research - Earth Surface*, 119, 644–664. <https://doi.org/10.1002/2013JF002897>
- Mesinger, F., DiMegoand, G., Kalnay, E., Mitchell, K., Shafran, P. C., Ebisuzaki, W., ... Shi, W. (2006). North American regional reanalysis. *Bulletin of American Meteorological Society*, 87, 343–360. <https://doi.org/10.1175/BAMS-87-3-343>
- Morales-Hernández, M., Sharif, M. B., Gangrade, S., Dullo, T. T., Kao, S.-C., Kalyanapu, A., ... Hodges, B. R. (2020). High performance computing in water resources hydrodynamics. *Journal of Hydroinformatics*, 22(5), 1217–1235.
- Moriasi, D. N., Arnold, J. G., Van Liew, M. W., Bingner, R. L., Harmel, R. D., & Veith, T. L. (2007). Model evaluation guidelines for systematic quantification of accuracy in watershed simulations. *American Society of Agricultural and Biological Engineers*, 50(3), 885–900. <https://doi.org/10.13031/2013.23153>
- MRLC (Multi-Resolution Land Characteristics Consortium). (2011). National Land Cover Database (NLCD). <https://www.mrlc.gov/data/nlcd-2011-land-cover-conus-0>.
- Nardi, F., Annis, A., Di Baldassarre, G., Vivoni, E. R., & Grimaldi, S. (2019). GFPLAIN250m, a global high-resolution dataset of Earth's floodplains. *Scientific Data*, 6, 180309. <https://doi.org/10.1038/sdata.2018.309>
- Nardi, F., Biscarini, C., Francesco, S. D., Manciola, P., & Ubertini, L. (2013). Comparing a large-scale DEM-based floodplain delineation algorithm with standard flood maps: The Tiber River basin case study. *Irrigation and Drainage*, 62(2), 11–19. <https://doi.org/10.1002/ird.1818>
- Nardi, F., Morrison, R. R., Annis, A., & Grantham, T. E. (2018). Hydrologic scaling for hydrogeomorphic floodplain mapping: Insights into human-induced floodplain connectivity. *River Research and Applications*, 34(7), 675–685. <https://doi.org/10.1002/rra.3296>
- Nardi, F., Vivoni, E. R., & Grimaldi, S. (2006). Investigating a floodplain scaling relation using a hydrogeomorphic delineation method. *Water Resources Research*, 42, W09409. <https://doi.org/10.1029/2005WR004155>

- Naz, B. S., Kao, S.-C., Ashfaq, M., Rastogi, D., Mei, R., & Bowling, L.-C. (2016). Regional hydrologic response to climate change in the conterminous United States using high-resolution hydroclimate simulations. *Global and Planetary Change*, 143, 100–117. <https://doi.org/10.1016/j.gloplacha.2016.06.003>
- Neal, J., Schumann, G., & Bates, P. (2012). A subgrid channel model for simulating river hydraulics and floodplain inundation over large and data sparse areas. *Water Resources Research*, 48, W11506. <https://doi.org/10.1029/2012WR012514>
- Nelson, B. R., Prat, O. P., Seo, D., & Habib, E. (2016). Assessment and implications of NCEP stage IV quantitative precipitation estimates for product intercomparisons. *Wea. Forecast*, 31, 371–394. <https://doi.org/10.1175/WAF-D-14-00112.1>
- Noh, S. J., Lee, J.-H., Lee, S., & Seo, D.-J. (2019). Retrospective dynamic inundation mapping of hurricane Harvey flooding in the Houston metropolitan area using high-resolution modeling and high-performance computing. *Water*, 11(3), 597. <https://doi.org/10.3390/w11030597>
- Nyaupane, N., S. Bhandari, Md. M. Rahaman, K. Wagner, A. Kalra, S. Ahmad, and R. Gupta (2018), Flood frequency analysis using generalized extreme value distribution and floodplain mapping for hurricane Harvey in Buffalo bayou, world environmental and water resources congress 2018: Watershed management, *Irrigation and Drainage, and Water Resources Planning and Management*, 364–375. <https://doi.org/10.1061/9780784481400.034>.
- Oubeidillah, A. A., Kao, S.-C., Ashfaq, M., Naz, B. S., & Tootle, G. (2014). A large-scale, high-resolution hydrological model parameter data set for climate change impact assessment for the conterminous US. *Hydrology and Earth System Sciences*, 18 (1), 67–84. <https://doi.org/10.5194/hess-18-67-2014>
- Pappenberger, F., Beven, K., Horritt, M., & Blazkova, S. (2005). Uncertainty in the calibration of effective roughness parameters in HEC-RAS using inundation and downstream level observations. *Journal of Hydrology*, 302(1–4), 46–69. <https://doi.org/10.1016/j.jhydrol.2004.06.036>
- Peña, F., & Nardi, F. (2018). Floodplain terrain analysis for coarse resolution 2D flood modeling. *Hydrology*, 5(4), 52. <https://doi.org/10.3390/hydrology5040052>
- Prat, O. P., & Nelson, B. R. (2015). Evaluation of precipitation estimates over CONUS derived from satellite, radar, and rain gauge data sets at daily to annual scales (2002–2012). *Hydrology and Earth System Sciences*, 19, 2037–2056. <https://doi.org/10.5194/hess-19-2037-2015>
- Rudorff, C. M., Melack, J. M., & Bates, P. D. (2014). Flooding dynamics on the lower Amazon floodplain: 1. Hydraulic controls on water elevation, inundation extent, and river-floodplain discharge. *Water Resources Research*, 50, 619–634. <https://doi.org/10.1002/2013WR014091>
- Sampson, C. C., Smith, A. M., Bates, P. B., Neal, J. C., Alfieri, L., & Freer, J. E. (2015). A high-resolution global flood hazard model. *Water Resources Research*, 51, 7358–7381. <https://doi.org/10.1002/2015WR016954>
- Scheel, K., Morrison, R. R., Annis, A., & Nardi, F. (2019). Understanding the large-scale influence of levees on floodplain connectivity using a Hydrogeomorphic approach. *Journal of American Water Resources Association*, 55, 413–429. <https://doi.org/10.1111/1752-1688.12717>
- Schumann, G. J. P., Neal, J. C., Voisin, N., Andreadis, K. M., Pappenberger, F., Phanthuwongpakdee, N., ... Bates, P. D. (2013). A first large-scale flood inundation forecasting model. *Water Resources Research*, 49, 6248–6257. <https://doi.org/10.1002/wrcr.20521>
- Sebastian, A., Lendering, K. T., Kothuis, B. L. M., Brand, A. D., Jonkman, S. N., van Gelder, P. H. A. J. M., ... Nespeca, V. (2017). *Hurricane Harvey report: A fact-finding effort in the direct aftermath of hurricane Harvey in the greater Houston region*. Delft: Delft University Publishers. http://pure.tudelft.nl/ws/files/31283193/TU_Delft_Texas_Hurricane_Harvey_Report_Phase_I_20171108.pdf
- Shin, S., Pokhrel, Y., & Miguez-Macho, G. (2017). High-resolution modeling of reservoir release and storage dynamics at the continental scale. *Water Resources Research*, 55, 787–810. <https://doi.org/10.1029/2018WR023025>
- Storey, A. L., & Talbott, M. D. (2009). Harris County Flood Control District: Hydrology and Hydraulics Guidance Manual. https://www.hcfcd.org/media/1999/hcfcd-hydrology-hydraulics-manual_03-2016.pdf.
- Sugarbaker, L. J., Constance, E. W., Heidemann, H. K., Jason, A. L., Lukas, V., Saghy, D. L., & Stoker, J. M. (2014). The 3D elevation program initiative—A call for action. *U.S. Geological Survey: Circular*, 1399, 35. <https://doi.org/10.3133/cir1399>
- Thornton, P. E., Running, S. W., & White, M. A. (1997). Generating surfaces of daily meteorological variables over large regions of complex terrain. *Journal of Hydrology*, 190, 214–251. [https://doi.org/10.1016/S0022-1694\(96\)03128-9](https://doi.org/10.1016/S0022-1694(96)03128-9)
- UNISDR (United Nations Office for Disaster Risk Reduction) (2015). *Making Development Sustainable: The Future of Disaster Risk Management, Global Assessment Report on Disaster Risk Reduction*, Geneva, Switzerland. https://www.preventionweb.net/english/hyogo/gar/2015/en/gar-pdf/GAR2015_EN.pdf.
- USACE (United States Army Corps of Engineers). (2012). *Water Control Manual: Addicks and Barker Reservoirs, Buffalo Bayou and Tributaries, San Jacinto River Basin, TX*, USACE Galveston District. <https://www.swg.usace.army.mil/Portals/26/docs/water%20control%20manual/2012%20water%20control%20manual.pdf>.
- Watson, K. M., Harwell, G. R., Wallace, D. S., Welborn, T. L., Stengel, V. G., & McDowell, J. S. (2018). Characterization of peak streamflows and flood inundation of selected areas in southeastern Texas and southwestern Louisiana from the August and September 2017 flood resulting from Hurricane Harvey: U.S. Geological Survey Scientific Investigations Report 2018-5070 (p. 44). <https://doi.org/10.3133/sir20185070>.
- Wing, O. E. J., Bates, P. D., Sampson, C. C., Smith, A. M., Johnson, K. A., & Erickson, T. A. (2017). Validation of a 30 m resolution flood hazard model of the conterminous United States. *Water Resources Research*, 53, 7968–7986. <https://doi.org/10.1002/2017WR020917>
- Wing, O. E. J., Sampson, C. C., Bates, P. D., Quinn, N., Smith, A. M., & Neal, J. C. (2019). A flood inundation forecast of hurricane Harvey using a continental-scale 2D hydrodynamic model. *Journal of Hydrology X*, 4, 100039. <https://doi.org/10.1016/j.jhydroa.2019.100039>
- Yamazaki, D., Baugh, C. A., Bates, P. D., Kanae, S., Alsdorf, D. E., & Oki, T. (2012). Adjustment of a spaceborne

DEM for use in floodplain hydrodynamic modelling. *Journal of Hydrology*, 436–437, 81–91. <https://doi.org/10.1016/j.jhydrol.2012.02.045>

Zheng, X., Maidment, D. R., Tarboton, D. G., Liu, Y. Y., & Passalacqua, P. (2018). GeoFlood: Large-scale flood inundation mapping based on high-resolution terrain analysis. *Water Resources Research*, 54, 10,013–10,033. <https://doi.org/10.1029/2018WR023457>

How to cite this article: Dullo TT, Gangrade S, Morales-Hernández M, et al. Simulation of Hurricane Harvey flood event through coupled hydrologic-hydraulic models: Challenges and next steps. *J Flood Risk Management*. 2021;14:e12716. <https://doi.org/10.1111/jfr3.12716>